A simplified drop breakage model for emulsion-producing fluidic devices: Application to fluidic oscillator, helical coil and vortex-based cavitation device

Chemical Engineering Research and Design 205 (2024) 733–747

Contents lists available at ScienceDirect

Chemical Engineering Research and Design

journal homepage: www.elsevier.com/locate/cherd

A simplified drop breakage model for emulsion-producing fluidic devices: Application to fluidic oscillator, helical coil and vortex-based cavitation device

Deepak K. Pandey, Abhijeet H. Thaker, Vivek V. Ranade *

Multiphase Reactors and Intensification Group, Bernal Institute, University of Limerick, Limerick V94T9PX, Ireland

ARTICLE INFO

Keywords:
Droplet size distribution
Sauter mean diameter
Cavitation
Shear
Dissipation rate

ABSTRACT

Droplet size distribution (DSD) is one of the key quality attributes of liquid–liquid emulsions. Various fluidic devices are used to generate emulsions. Most of the currently available models for estimating DSD are complicated to implement and computationally expensive. In this work, we have developed a simplified drop breakage model that is easy to implement and computationally inexpensive. This model approximates DSDs in three droplet populations, each characterised by a mean diameter. The developed drop breakage model was applied to simulate Sauter mean diameters of oil-in-water emulsions generated using three fluidic devices covering a broad range of shear rates and droplet sizes namely: vortex-based cavitation device (VD), helical coil (HC), and fluidic oscillator (FO). The variation of DSD with the number of passes (n_p) through the emulsion-producing fluidic devices was measured experimentally. The Sauter mean diameter (d_{32}) and number of droplets (n) in each population were estimated from the measured DSD data. The procedure to estimate model parameters is presented. The simplified breakage model presented here was able to simulate the influence of the number of passes and operating conditions on Sauter mean diameter as well as breakage efficiency. VD was found to exhibit the highest drop breakage efficiency. FO was found to be a preferred choice for low (< 20 J/kg) energy consumption, HC for the middle range (20 – 100 J/kg) and VD for the higher (> 100 J/kg) range of energy consumption. The developed approach and model provide a simplified way of simulating the Sauter mean diameters of emulsions for a variety of emulsion-generating devices.

1. Introduction

Various products in personal care (cosmetics, beauty care), home care (paints, room fresheners) and food (dairy, ice cream) industries are formulated using liquid-liquid emulsions. One of the most important critical quality attributes (CQA) in emulsions is the droplet size distribution (DSD), which affects other qualities like rheology, appearance, stability etc. Consequently, significant effort has been dedicated to developing techniques for creating emulsions with the intended droplet size distribution (DSD). Based on the product applications, emulsions are distinguished into three categories: macro-emulsions (drop size: 1−100 μm), micro-emulsions (drop size: 10−100 nm), and nano-emulsions (drop size: 20–500 nm) (Gupta et al., 2016; Gohtani and Prasert, 2014; Karunaratne et al., 2017). A variety of emulsion preparation techniques and equipment are available, including impeller vessels (Groeneweg et al., 1994; Becker et al., 2013; Khalil et al., 2010) rotor-stators (Gupta et al., 2016; Wang et al., 2008; Li and Xiang, 2019) high-pressure homogenizers (Li and Xiang, 2019; Maindarkar et al., 2014) colloid mills (Maindarkar et al., 2014; Perrier-Cornet et al., 2005) ultrasonics (O'Sullivan et al., 2015; Servant et al., 2001) hydrodynamic cavitation (Parthasarathy et al., 2013; Tang et al., 2013; Ashokkumar et al., 2011; Ramisetty et al., 2014; Zhang et al., 2016; Carpenter et al., 2017; Fesenko et al., 2018) membranes and microchannels (Urban et al., 2006) etc. The ultrasonication system and membranes are used extensively in laboratory-scale or development systems. The main disadvantages of these equipment systems are high power requirements and scale-up difficulties. Stirred tanks, high-pressure homogenizers or rotor-stators and hydrodynamic cavitation are industrial emulsion production systems (Urban et al., 2006). The helical coil (HC) and fluidic oscillator (FO) deserve mention as innovative solutions in this landscape. The helical coil configuration offers benefits like intensified mixing and shear, enabling controlled droplet size reduction (Dillon et al., 2020). The fluidic oscillator leverages its oscillatory flow patterns

* Corresponding author.
E-mail address: vivek.ranade@ul.ie (V.V. Ranade).

https://doi.org/10.1016/j.cherd.2024.04.038
Received 10 February 2024; Received in revised form 13 April 2024; Accepted 17 April 2024
Available online 21 April 2024

Nomenclature

a	fixed parameter, -
b_1	fixed parameter, -
b_2	fixed parameter, $m^{4/3}\ s^{-3}$
C_1	calculated parameter, $m^{-2/3}$
C_2–C_3	fixed parameters, -
d_1, d_2, d_3	maximum mean drop diameters of group 1, group 2, and group 3, μm
$d_{1min}, d_{2min}, d_{3min}$	minimum mean drop diameters of group 1, group 2, and group 3, μm
d_{32}	Sauter mean diameter, μm
e	fixed parameter, -
k_{12}	drop breakage rate from droplet group 1 to group 2, s^{-1}
k_{13}	drop breakage rate from droplet group 1 to group 3, s^{-1}
k_{23}	drop breakage rate from droplet group 2 to group 3, s^{-1}
k_j	effective rate of equilibration of j group of droplets, $m^{1\text{-}a}/s$
$n_1 - n_3$	population of droplets with diameter d_1 to d_3 at the beginning of the device, -
$n_1^{'} - n_3^{'}$	population of droplets with diameter d_1 to d_3 at the end of the device, -
n	number of drops per unit volume, -
n_p	number of passes, -
ΔP	pressure drop across the device, kPa
Q,q	flow rate, m^3/s
t	flow time, s
V	volume of emulsion in the experimental loop including piping, device, holding tank, m^3
w	volume fraction, -

Greek letters

α_j^D	ratio of $\varepsilon/\varepsilon_{eff,j}$, -
α	volume fraction, -
ρ	density, kg/m^3
μ	viscosity, kg/m-S
σ	interfacial tension, N/m
η	breakage efficiency, %
ε	energy dissipation rate per unit mass in the device, m^2/s^3
$\varepsilon_{eff,j}$	effective energy dissipation rate of j group, m^2/s^3
ε_1	Effective energy dissipation rate for eddies larger than d_1, m^2/s^3
ε_2	Effective energy dissipation rate for eddies larger than d_2, m^2/s^3
$\varepsilon_{cav.}$	Effective energy dissipation rate by collapsing cavities, m^2/s^3
$\bar{\varepsilon}$	average energy dissipation rate per unit mass in the device, m^2/s^3
θ	residence time, s
τ	residence time in the holding tank, s

Subscript

c	continuous phase
d	dispersed phase
D	device
j	j group of droplets
o	oil

Acronyms

CFD	computational fluid dynamics
DSD	drop size distribution
FBRM	focused beam reflectance measurements
FO	fluidic oscillator
HC	helical coil
LPM	litre per minute
MS	mastersizer
PDF	probability density function
RO	rapeseed oil
VD	vortex diode
v*DSD*	volume-based DSD

to facilitate efficient mixing and emulsification (Tesař et al., 2013; Ghanami and Farhadi, 2019a; Li and Barrow, 2017; Hanotu et al., 2013).

The droplet size distribution of emulsions is controlled primarily by droplet breakage since in many applications, coalescence is suppressed by using surfactants. A quantitative and qualitative understanding of droplet breakage is essential for the development of models for simulating droplet size distributions of emulsions. It is important to predict how the dispersed phase size distribution evolves and how fast the break-up processes occur (Alopaeus et al., 2002a; Coulaloglou and Tavlarides, 1977a). Information about the dynamics of the breakup process leads to improved control of the interfacial area for mass, heat and momentum transfer (Andersson et al., 2011; Moilanen et al., 2008). The mathematical framework widely used to investigate multiphase systems involving the breakup of the dispersed phase is computational fluid dynamics (CFD) coupled with the population balance models (PBM) (Marchisio et al., 2013; Petitti et al., 2013; Xiao et al., 2017; Nauha et al., 2018; Thaker and Ranade, 2021a). Extensive efforts have been spent on the development of mathematical models for simulating droplet breakup processes in the past few decades (Lasheras et al., 2002; Solsvik et al., 2013; Liao and Lucas, 2009; Guo et al., 2017). A typical approach involves conceptualizing droplet fragmentation as the interaction between a fluid element and a turbulent pattern, determined by the frequency and likelihood of their engagements. This methodology has been widely used to develop various droplet breakage models (Luo and Svendsen, 1996; Coulaloglou and Tavlarides, 1977b; Konno et al., 1980; Alopaeus et al., 2002b; Andersson and Andersson, 2006; Han et al., 2011; Solsvik and Jakobsen, 2016; Solsvik et al., 2016). Successful application of this methodology requires reliable and accurate simulation of underlying mean and turbulence flow field and resulting droplet breakage processes. Invariably, these models involve non-linear and strongly interlinked partial differential equations, often requiring significant computational resources and time. Calibrating and validating these models can be challenging and require extensive experimental data. The uncertainties involved in estimating various parameters often raise some questions about the predictive ability of these models.

This study is aimed at developing a simplified model for simulating drop breakage and the resulting DSD in emulsion-producing fluidic devices. For reducing computational demands, typically, method of moments (MOM) or its variants are used, instead of fully resolved solution of population balance models. In the MOM, typically first three moments are solved which are related to the number, size and area of droplets. However, the application and interpretation of MOM to bi-modal distribution is not straightforward (Petitti et al., 2010). Hydrodynamic cavitation device considered in this work is expected to generate bi-modal DSD because of highly localized events of cavity collapse, as confirmed by experiments (Thaker and Ranade, 2022a). Considering the difficulties in extending the MOM framework and interpretation for the bi-modal DSD, we developed a simplified model which will provide with more intuitive and easier to interpret results for a wide range of scenarios (Petitti et al., 2010; Thaker and Ranade, 2022a; Kamp et al., 2012; Maaß and Kraume, 2012a; Pandey et al., 2023). Here, the primary simplification is to represent the continuous DSD by the sum of three distinct droplet populations, each characterized by a mean diameter as schematically shown in Fig. 1. If necessary, it may be possible to

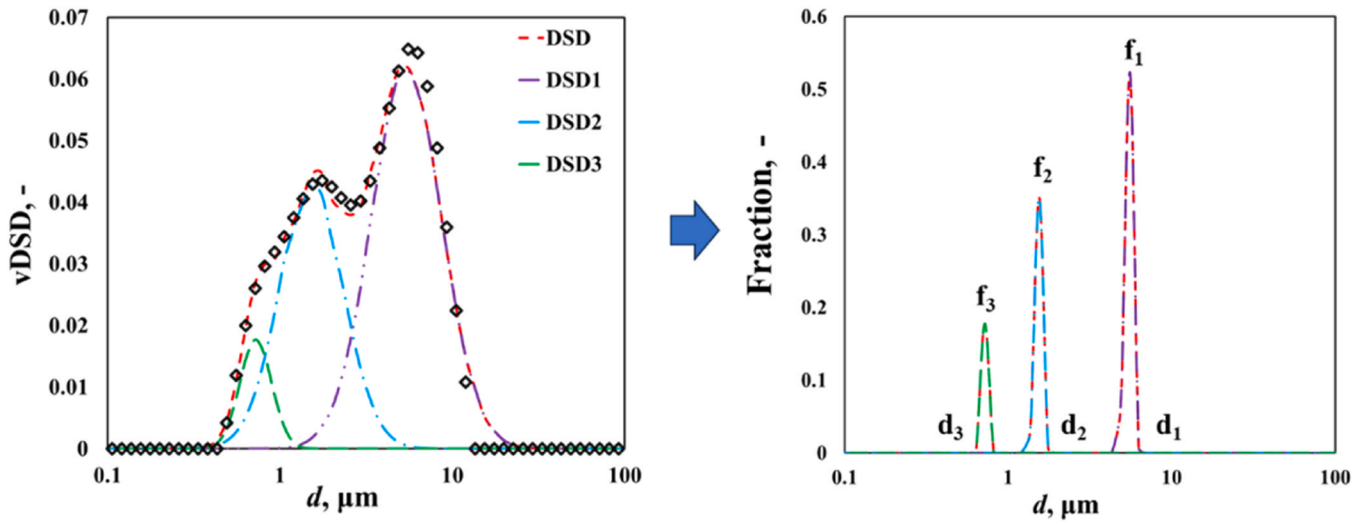

Fig. 1. : Left – typical volume-based DSD of emulsion (vDSD) which may be represented by the sum of three log-normal distributions as shown by dashed lines; Right – same vDSD is represented by the sum of three mono-dispersed droplet populations each characterised by mean diameters, d_1, d_2 and d_3.

reconstruct detailed DSD from these three mean diameters by making suitable approximations about the variance of DSD. More details of the proposed simplified physical picture are discussed in Section 3.1. Based on this simplified representation, we have developed a model considering two modes of droplet breakage: equilibration of drop size because of the long exposure to shear and drop breakage as envisaged by typical breakage models like the Laakkonen breakage model (Maaß and Kraume, 2012b; Laakkonen et al., 2007; Matiazzo et al., 2020). The model was applied and evaluated using the DSD of emulsions produced by three fluidic devices covering a wide range of shear rates, droplet diameters and two breakage mechanisms (shear and cavitation) namely: FO, HC and vortex-based cavitation device (VD). These fluidic devices are simple to manufacture, do not have any moving parts, and are increasingly being used for making emulsions. The oil-in-water emulsions were generated using three fluidic devices. The experiments, model development and application are discussed in Sections 2, 3 and 4 respectively. The presented approach, models and results will be useful for selecting appropriate fluidic devices and operating parameters for realising emulsions with desired DSD and Sauter mean diameter.

2. Experiments

2.1. Experimental setup and procedure

The multiple-pass experiments were performed to generate liquid−liquid emulsions using VD, HC and FO. Fig. 2 shows the schematic of the experimental setup. Additional details of the experimental set-up are included in Section S1 of the supplementary information. The dimensions of the VD and FO used in this work are the same as reported by Simpson and Ranade (Simpson and Ranade, 2019) and Madane et al. (2023); Madane and Ranade (2022) respectively. The length and diameter of the helical coil used in this work were 4000 mm and 4 mm respectively. The pressure drop values were measured in triplicate and the measured values were found to be within ±3 %. The flow rate through fluidic devices was also measured in triplicate using a flow meter and within ±2 %. It is in principle possible to develop a computational fluid dynamics based model for simulating flow and therefore pressure drop characteristics of the considered devices (Ranade, 2022; Ranade and Utikar, 2022). However, to be consistent with the approach for developing the simplified model, we developed simple empirical correlations based on experimental data for estimating pressure drop and mean energy dissipation rates in the considered devices The pressure drop values at different flow rates through these devices were

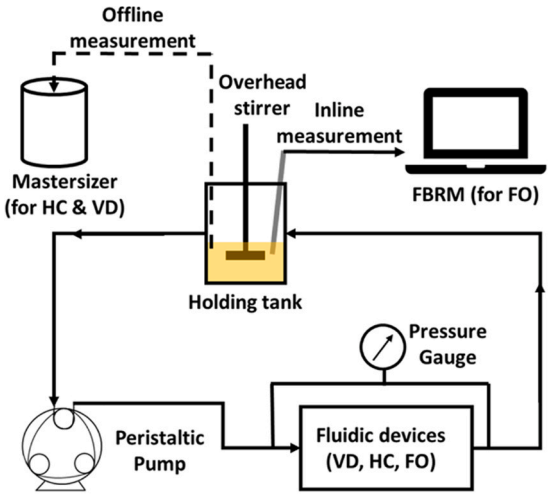

Fig. 2. Schematic of experimental set-up used for generating oil in water emulsions using the fluidic devices (Vortex based cavitation device [VD], Helical coil [HC] and Fluidic Oscillator [FO]).

measured and a correlation for each of the considered fluidic devices (FO, HC, VD) was obtained as:

$$\Delta P = b_1 \quad q^e \tag{1}$$

Where ΔP is the pressure drop across the device, kPa and q is the flow rate, LPM. In this work, the values of b_1 was found to be 150 for VD, 90 for HC and 2 for FO, respectively. The value of e was found to be 2 for VD, 1.6 for HC and 1.5 for FO. Additional details of the devices are included in the supplementary information (Section S2). For the Reynolds number calculation, it is essential to select appropriate characteristic velocity and length scales. For VD, throat diameter was used as a characteristic length scale and area of the throat was used for calculating the velocity scale. For HC, the internal diameter (ID) of the tube was used as the characteristic length scale; the velocity scale was obtained from the flow rate and area calculated using the tube ID. For FO, the hydraulic diameter of the rectangular inlet was used as a characteristic length scale and the inlet area and flow rate was used to calculate characteristic velocity. The Reynolds numbers corresponding to experiments carried out in this work are listed in Table 1. It can be seen that the Reynolds number considered in this work falls in the range of $\sim 10^3$

Table 1
Operating conditions (and derived quantities) used with FO, HC, VD Device dimensions are listed in Section S2 of supplementary information.

S. No.	Fluidic device	V_D x 10^5 (m^3)	ΔP (kPa)	q x 10^5 (m^3/s)	$\bar{\varepsilon}$ (m^2/s^3)	θ_D (s)	τ (s)	d (m)	V (m/s)	Re (-)
1	Fluidic oscillator (FO)	6.12	1.8	1.67	0.5	3.67	30	0.0045	1.05	4706.28
			6.4	3.58	4	1.70	13.95		2.25	10,118.47
			10.6	5.00	9.3	1.22	10		3.14	14,118.81
2	Helical coil (HC)	5	96.7	1.67	28	3.00	30	0.004	1.33	5294.57
			130.5	2.13	49	2.34	23.44		1.70	6777.02
			170	2.63	79	1.89	18.99		2.10	8365.39
3	Vortex diode (VD)	0.07	50	1.06	797	0.07	47.17	0.003	1.50	4489.78
			150	1.71	3857	0.04	29.24		2.42	7242.95
			250	2.24	8421	0.03	22.32		3.17	9487.84

to 10^4. For cavitating flow, the Euler number was shown to be proportional to square of the characteristic velocity scale over the considered range of Reynolds numbers (Thaker and Ranade, 2022a). For HC and FO, considering the intermediate range of Reynolds number, the values of e was found to be lower than two.

The emulsions were generated using 5 and 15 vol% rapeseed oil (RO, $\rho_o = 915$ kg/m^3, $\mu_o = 6.2 \times 10^{-2}$ Pa s) procured from a local store (brand: Newgrange Gold) in demineralized water ($\rho_A = 997$ kg/m^3, $\mu_A = 7.972 \times 10^{-4}$ Pa s). The addition of 2 wt % TWEEN 20 (sourced from MP Biomedicals, LLC, France) surfactant was used for the RO in the water system to prevent drop coalescence (Thaker and Ranade, 2023). A total volume of 500 ml was used in the holding tank for experimentation with the emulsion-producing devices. The rapeseed oil-in-water pre-emulsion was generated by adding 5 % and 15 % (by volume) of the oil in water and using an overhead stirrer (IKA-Werke) operated at 600 rpm. Agitation of 15 min was found to be adequate for generating pre-emulsion (Thaker and Ranade, 2022b) at 600 rpm. Agitation of 15 min was found to be adequate for generating pre-emulsion (Thaker and Ranade, 2022b). The pre-emulsion was then pumped through the fluidic devices using the peristaltic pump (Longer BT600−2 J). Initially experiments were carried to quantify the possibility of drop breakage due to the action of peristaltic pump. The DSD of pre-emulsion and the DSD at the outlet of the pump at different number of passes through the pump (without fluidic device in the loop) were measured and it was confirmed that droplet breakage caused by the peristaltic pump is negligible (see Figure S4 of supplementary information for more details). After establishing this, the experiments were carried out by setting the desired pressure drop across the device by adjusting the rpm of the peristaltic pump which varies the flow rate through the device. Experiments were carried out up to 200 passes through the emulsion devices (number of passes through the fluidic device, $n_p = qt/V$ where q is the flow rate through the fluidic device, V is the volume of emulsion in the experimental loop including piping, device, and holding tank, and t is flow time). The pressure drop, flow rate, volume of the device (V_D), residence time in the emulsion device (θ_D) and residence time in the holding tank (τ) used in this work are listed in Table 1 respectively.

For emulsions generated using FO, focussed beam reflectance measurement (FBRM) was used to analyse DSD. Thaker and Ranade (Thaker and Ranade, 2022b) have reported that the DSD results obtained from FBRM and mastersizer (MS) are the same for droplets larger than 1 μm. Since FO does not reduce the drop size below 25 μm for any conditions considered in this work, the use of FBRM for FO is adequate. However, HC and VD were found to generate emulsions of droplet sizes smaller than 1 μm and therefore MS was needed instead of FBRM for analysing DSD. FBRM measures chord length distributions (CLD) which were converted to DSDs using the methodology developed by Pandit and Ranade (Pandit and Ranade, 2016). The details of DSD measurements are provided in Section S4 of supplementary information. The experiments were repeated three times and error bars were quantified based on these triplicate experiments. Typically, the errors were less than 10 % in the triplicate vDSD measurements.

2.2. Processing of experimental data

The measured DSDs are represented as the sum of three droplet populations ($j = 1, 2, 3$) represented by three log-normal distributions:

$$f(d) = \sum_{j=1}^{3} w_j f_j(d) \quad \text{where } f_j(d) = \frac{1}{d\sigma_j\sqrt{2\pi}} e^{\left[-\frac{\left(\ln d - \mu_j\right)^2}{2\sigma_j^2}\right]} \tag{2}$$

Where d is a droplet diameter, w_j are volume fractions of j^{th} log-normal function, μ_j is the mean of the j^{th} log-normal function, $f_j(d)\Delta d$ is a volume fraction of oil droplets of j^{th} population having diameters between d and $d + \Delta d$, and $\sigma_j^2$is the variance of j^{th} log-normal function. σ_j is the standard deviation of j^{th} log-normal function. The sum of volume fractions of three droplet populations is one:

$$\sum_{j=1}^{3} w_j = 1 \tag{3}$$

Eq. (2) was used to describe the experimentally measured DSD by optimising a set of eight parameters: means ($\mu_1, \mu_2 and \mu_3$) and standard deviations ($\sigma_1, \sigma_2 and \sigma_3$) for each of the three distributions and two volume fractions ($w_1$and w_2). A non-linear optimisation tool embedded in MS Excel was used to obtain values of these eight parameters by minimising the sum of squares of errors. Based on the fitted parameters, the mean of the j^{th} log normal distribution d_j and number of droplets of each of these three mono-dispersed droplet populations were calculated as (refer Section S4 of supplementary information):

$$n_j = \frac{6\alpha_o}{\pi}\left(\frac{w_j}{d_j^3}\right) \text{ where } d_j = e^{\left(\mu_j + \frac{\sigma_j^2}{2}\right)} \tag{4}$$

Where α_O is the overall volume fraction of oil in water, d_j is the mean drop diameter of the group j. The number of droplets of three representative droplet populations was then modelled using the simplified breakage model discussed in Section 3.

3. Mathematical model

3.1. Key concepts and their mathematical representation

3.1.1. Physical picture of drop breakage model

For the development of the simplified drop breakage model for the emulsion-producing fluidic devices, it is necessary to represent the physical processes causing droplet breakage in these devices. When the emulsion is passed through fluidic devices, each pass results in drop breakage and droplet size distribution shifts towards lower-size droplets. This process of droplet breakage is shown schematically in Fig. 3a. It should be noted that the interaction of turbulent eddies and droplets, and the possibility of resulting droplet breakage is strongly influenced by scales of interacting eddies and droplets. The presence of cavitation

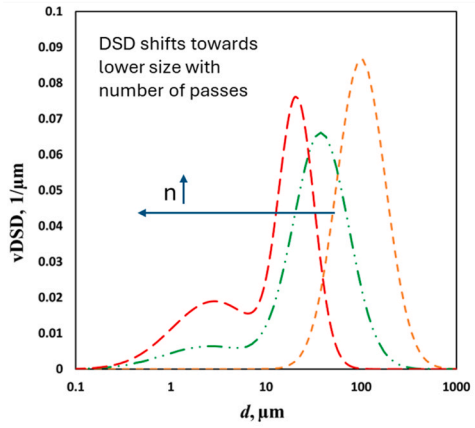

(a) Typical droplet size distributions and influence of the number of passes through the device

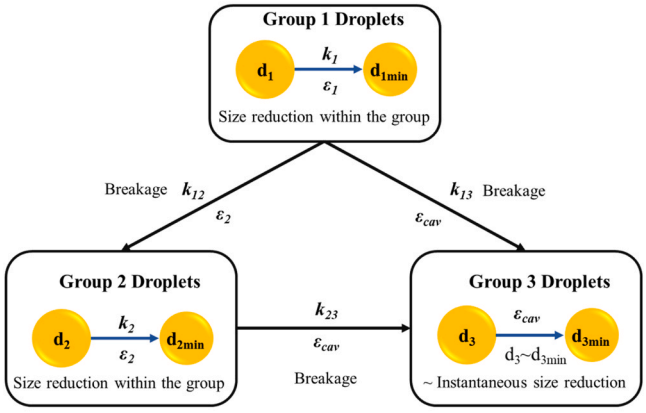

ε_1: Effective energy dissipation rate for breakage of droplets of size larger than d_{1min}

ε_2: Effective energy dissipation rate for breakage of droplets of size larger than d_{2min}

(b) Schematic of droplet breakage processes considered in simplified drop breakage model

Fig. 3. Droplet size distribution and simplified drop breakage model.

generates intense localized shear and energy dissipation which are orders of magnitude higher than that prevailing in other devices. Therefore, the droplet sizes generated in VD are much smaller than the other two devices (FO and HC). As discussed in the introduction (Section 1), in this work, the overall DSD is represented in terms of three monodispersed droplet populations. These three droplet populations are characterised by mean diameters. The overall droplet breakage processes while transforming pre-emulsion into emulsion by multiple passes through fluidic devices are shown schematically in Fig. 3b.

The droplet population indicated by Group 1 represents the pre-emulsion droplet population characterised by the mean initial (at time $t = 0$ or at $n_p = 0$) droplet diameter, d_1. Note that two distinct breakage processes are envisaged in this simplified model. The first one occurs within each group – this is like an equilibration within the group because of the extended exposure to effective shear or energy dissipation rate. As the droplet population in a group is exposed to fluid shear and turbulence in fluidic devices, the characteristic droplet diameter representing this group j, d_j reduces with the number of passes through the device and eventually attains minimum droplet diameter characterising Group j, d_{jmin}. This minimum diameter is dictated by physical properties (viscosity of dispersed and continuous phase and interfacial tension) and characteristic energy dissipation rate/ shear caused by the eddies capable of breaking droplets of size larger than d_{jmin} (denoted by ε_j). It should be noted that this change in the characteristic diameter of Group j droplets is like approaching an equilibrium droplet diameter if exposed to ε_j for an infinite time. This equilibration process and resulting adjustment in droplet size needs to be and is treated differently in the developed model. The rate of achieving this equilibration is denoted by k_j. In the present work, DSD is represented by considering three monodispersed droplet populations. The $d_{1\,min}$, $d_{2\,min}$ and $d_{3\,min}$ are minimum droplet diameters of these three groups if the droplet population is exposed to corresponding characteristic energy dissipation rates, ε_1, ε_2 and ε_3 (denoted by ε_{cav} to characterise the role of collapsing cavities) respectively. For Group 3 droplets, the Rayleigh Plesset equation-based cavity dynamics simulations (Pandit et al., 2021) indicate that the effective energy dissipation rate, ε_{cav}, caused by collapsing cavities is very high ($\sim 10^7$ m^2/s^3). Therefore, the equilibration rate for Group 3 may be assumed to be very high resulting in a nearly instantaneous conversion of d_3 to $d_{3\,min}$. This is assumed and therefore d_3 was set to $d_{3\,min}$ and the equilibration step for Group 3 (k_3) is not considered in the model.

Besides this equilibration process, the droplets of Groups 1 and 2 may undergo breakage either because of prevailing shear in the device or caused by collapsing cavities. These droplet breakage processes are shown schematically in Fig. 3b. The breakage rates of Group 1 droplets to form Group 2 and Group 3 droplets are characterised by two distinct breakage rates, k_{12} and k_{13}, representing the breakage rate of Group 1 droplets to form Group 2 and Group 3 droplets respectively. In addition to this, there is a possibility that the droplets from Group 2 may undergo further breakage to form droplets of Group 3. The effective rate of this breakage is represented by k_{23}. The proposed modelling of these envisaged breakage processes is discussed in the following section.

3.1.2. *Mathematical representation of proposed breakage processes*

The equilibration process during exposure to prevailing shear and energy dissipation rates of droplets within each group may be modelled as:

$$\frac{dd_j}{dt} = -k_j(d_j - d_{jmin})^a \tag{5}$$

Where subscript j indicates j^{th} group and d_{jmin} is the minimum drop diameter that may be attained within the group j. Please note that Eq. (5) is used only for the first two droplet populations (j=1, 2). By using the conservation of mass, Eq. (5) may be written as:

$$\frac{dn_j}{dt} = \frac{3n_j}{d_j}k_j(d_j - d_{jmin})^a \tag{6}$$

Where n_j is the number of droplets in Group j. The rate constants, k_j is the effective rate of equilibration with units as m$^{1\text{-}a}$/s. Preliminary experiments with pre-emulsion (Group 1 droplets) were carried out and the data was used to estimate the variation of d_1 with time (or in other words, the number of passes, n_p). The observed variation of d_1 was used to estimate the parameter, a. The value of a was varied as 2, 3 and 4. A non-linear optimisation tool embedded in MS Excel was used to obtain values of k_1 by minimising the sum of squares of errors between the diameter variation obtained from log-normal fitting for various passes. These results are shown in Fig. 4. It can be seen from Fig. 4 that $a = 3$ represents the experimental data well. The value of parameter a was fixed at 3 for all subsequent calculations.

More details of the application of the model to specific devices are discussed in Section 3.2

For representing the inter-group droplet breakage, the rate of droplet breakage is assumed to be linearly proportional to the number of droplets of the group that is breaking. For example, for Group 1, the change in the number of Group 1 droplets because of breakage to Group 2 and 3 may be represented as:

$$\frac{dn_1}{dt} = -k_{12}n_1 - k_{13}n_1 \tag{7}$$

Where, k_{ji} is a breakage rate of Group j to Group i. The inter-group droplet breakage rates may be modelled using established breakage models. In this work, we propose to use the model of Laakkonen (Matiazzo et al., 2020) for estimating droplet breakage rates, k_{12}, k_{13} and k_{23}

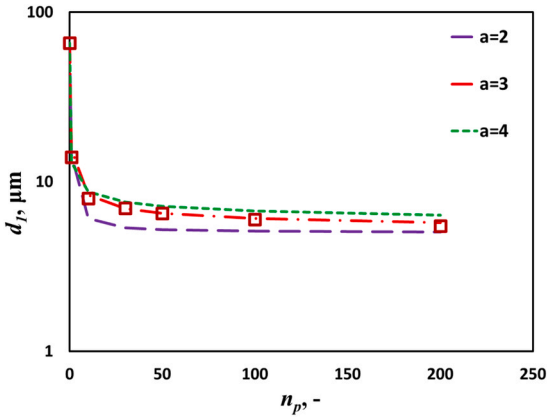

Fig. 4. Sensitivity of the simulated results with parameter a $k_1 = 4.10\text{x}10^{-3}$ m^{-1} s^{-1} at $a = 2$, $k_1 = 2\text{x}10^{-4}$ m^{-2} s^{-1} at $a = 3$, $k_1 = 2\text{x}10^{-4}$ m^{-3} s^{-1} at $a = 4$.

as:

$$k_{ji} = C_1 \quad \varepsilon_i^{1/3} \operatorname{erfc}\left(\sqrt{C_2\frac{\sigma}{\rho_c \varepsilon_i^{2/3} d_j^{5/3}} + C_3\frac{\mu_d}{\sqrt{\rho_c \rho_d}\quad \varepsilon_i^{2/3} d_j^{5/3}}}\right) \tag{8}$$

Where, k_{ji} is a breakage rate of Group j to Group i, d_j is the diameter of the breaking drop (Group j) and ε_i is an effective energy dissipation rate for breaking droplets larger than d_{imin}. $\mu_d$is the viscosity of oil (kg/m-s), ρ_c is the density of water (kg/m^3), ρ_d is the density of oil (kg/m^3) and σ is surface tension (N/m). C_1, C_2 and C_3 are the parameters of Laakkonen breakage model (Laakkonen et al., 2006). The values of parameters C_2 and C_3 were set to 0.04 and 0.01 respectively as recommended in (Laakkonen et al., 2006). The value of the parameter C_1 is system-specific, has significant influence on simulated results and need to be obtained from experimental data (Gemello et al., 2019; Thaker and Ranade, 2021b). The procedure for estimating and obtaining the values of C_1 is discussed in Section 4.1. The envisaged simplified breakage processes and their corresponding mathematical representation were used to develop a specific model for simulating drop breakage in three emulsion-producing fluidic devices discussed in Section 2.

3.2. Application of the model to fluidic devices used in this work

The basic concepts of the proposed model discussed in Section 3.1 are applied to simulate the experimental set-up (Fig. 2) used in the present work for producing emulsions using three fluidic devices. For the considered set-up, the model equations can be written as:

$$V\frac{dn_j}{dt} = \frac{3n_j}{d_j}k_j(d_j - d_{jmin})^3 + Q\left(n_j^{'} - n_j\right) \tag{9}$$

Where V and Q are the volume of emulsion in the holding tank and flow rate through the fluidic device respectively. It should be noted that for Group 3 (j=3), the first term on the right-hand side of Eq. (9) is absent because $d_j = d_{jmin}$. The term, $\left(n_j^{'} - n_j\right)$ represents the change in the number of droplets in Group j, because of the drop breakage that occurred in the device due to various phenomena (shearing, cavitation etc). Since Group 1 is the group with a droplet of bigger size (d_1), the droplets break from it and contribute to Group 2 and Group 3. Moreover, the number of droplets (n_1) from Group 1 breaks to form Group 2 and Group 3 with the breakage rates k_{12} and k_{13}. Similarly, there is a change in the number of droplets of Group 2 because of the contribution of drop breakage from Group 1 and the breakage of droplets from Group 2 to form droplets of Group 3. The change in number of droplets of group 3 is because of droplets contributed from Group 1 and Group 2.

$$V_D\frac{dn_1^{'}}{dt} = -Q\left(n_1^{'} - n_1\right) + V_D\left(-k_{12}n_1^{'} - k_{13}n_1^{'}\right) \tag{10}$$

$$V_D\frac{dn_2^{'}}{dt} = -Q\left(n_2^{'} - n_2\right) + V_D\left[k_{12}n_1^{'}\left(\frac{d_1}{d_2}\right)^3 - k_{23}n_2^{'}\right] \tag{11}$$

$$V_D\frac{dn_3^{'}}{dt} = -Q\left(n_3^{'} - n_3\right) + V_D\left[k_{13}n_1^{'}\left(\frac{d_1}{d_3}\right)^3 + k_{23}n_2^{'}\left(\frac{d_2}{d_3}\right)^3\right] \tag{12}$$

where V_D is the volume of the fluidic device used for producing emulsions. The residence time in the fluidic device (θ_D) is the order of magnitude smaller than the time scale of producing emulsions. A quasi-steady state approximation may be therefore be used for simplifying the model equations. A detailed derivation and basis for the quasi-steady state approximation is provided in Section S5 of the supplementary information. With this assumption, the LHS of Eqs. (10) to (12) may be set to zero to obtain:

$$Q\left(n_1^{'} - n_1\right) = V_D\left(-k_{12}n_1^{'} - k_{13}n_1^{'}\right) \tag{13}$$

$$Q\left(n_2^{'} - n_2\right) = V_D\left[k_{12}n_1^{'}\left(\frac{d_1}{d_2}\right)^3 - k_{23}n_2^{'}\right] \tag{14}$$

$$Q\left(n_3^{'} - n_3\right) = V_D\left[k_{13}n_1^{'}\left(\frac{d_1}{d_3}\right)^3 + k_{23}n_2^{'}\left(\frac{d_2}{d_3}\right)^3\right] \tag{15}$$

Substituting Eqs. (13–15) in Eq. (9) and by replacing time (t) with the number of passes ($n_p = \frac{Qt}{V}$), we get the final set of model equations as:

$$\frac{dd_j}{dn_p} = -k_j\tau(d_j - d_{jmin})^3 \text{for } j = 1, 2 \tag{16}$$

$$\frac{dn_1}{dn_p} = \frac{3n_1}{Vd_1}k_1\tau(d_1 - d_{1\min})^3 - n_1\left[\frac{(k_{12}+k_{13})\theta_D}{1+(k_{12}+k_{13})\theta_D}\right] \tag{17}$$

$$\frac{dn_2}{dn_p} = \frac{3n_2}{Vd_2}k_2\tau(d_2 - d_{2\min})^3 + \left[\frac{1}{(1+\theta_D k_{23})}\left(\frac{\theta_D k_{12} n_1\left(\frac{d_1}{d_2}\right)^3}{1+(k_{12}+k_{13})\theta_D}\right)\right] - \frac{\theta_D k_{23} n_2}{(1+\theta_D k_{23})} \tag{18}$$

$$\frac{dn_3}{dn_p} = \frac{3n_3}{Vd_3}k_3\tau(d_3 - d_{3\min})^3 + \left[\frac{\theta_D k_{13} n_1\left(\frac{d_1}{d_3}\right)^3}{1+(k_{12}+k_{13})\theta_D} + \frac{\theta_D k_{23}\left(\frac{d_2}{d_3}\right)^3}{(1+\theta_D k_{23})}\left[\frac{\theta_D k_{12} n_1\left(\frac{d_1}{d_2}\right)^3}{1+(k_{12}+k_{13})\theta_D} + n_2\right]\right] \tag{19}$$

Where τ is the residence time of the holding tank $\left(\frac{V}{Q}\right)$, θ_D is the residence time in the emulsion device $\left(\frac{V_D}{Q}\right)$. Eqs. (16–19), represent the change in the droplet density with the number of passes and it includes the change in drop diameter, the flow rate through the emulsion device, drop breakage rates and residence time in the emulsion device.

4. Results and discussions

The estimation of model parameters is first discussed in the following sub-section. The application to three fluidic devices is then discussed in the subsequent sub-sections.

4.1. Estimation of model parameters

There are primarily six unknown variables ($d_j, n_j with\ j = 1, 3$) and corresponding five ordinary differential equations (ODEs, Eqs. 16–19) and one algebraic equation ($d_3 = d_{3\min}$). The initial conditions at $n_p = 0$, can be specified from the measured DSDs of pre-emulsion. As discussed in Section 2.2, measured DSD was represented by the fitting sum of three log-normal distributions. The three mean diameters obtained from these three fitted log-normal distributions were assigned as the initial diameters of the three groups. In case of a monomodal DSD, the values of w_j for two distributions become zero. It should be noted that when the value of w_j is zero, it is not possible to calculate d_j. Therefore, for the monomodal case, d_1 was obtained from the pre-emulsion (zero pass condition) and d_2 and if applicable, d_3 were obtained from the DSD measured after passes through fluidic devices. The corresponding initial number of droplets was calculated using Eq. (4). Moreover, d_j for other passes, that is 10 and 100 passes also used in this work for the validation purposes of d_j and d_{32}. In the present work, the model equations were solved using MATLAB (R2022b) with the ode45 solver. Appropriate care was taken to ensure that the results obtained were independent of specified values of tolerances. To solve the model equations, it is essential to estimate the following parameters:

- Three minimum diameters: d_{jmin}
- Two equilibration rate constants: k_j
- Three breakage rate constants: k_{12}, k_{13}, k_{23}

If the experimental data on DSD is available, the droplet diameters obtained after many passes (~200) can be used as d_{jmin}. Alternatively, the minimum droplet diameter may be obtained from the effective turbulent energy dissipation rates. The droplet breakage occurs via interactions with the eddies with a length scale smaller than or equal to the droplet size (d_j) having adequate energy to break the drops (Luo and Svendsen, 1996; Lehr et al., 2002; Razzaghi and Shahraki, 2016). The large eddies will simply transport the droplets. The breakage caused via interaction with turbulent eddies will continue and eventually approach the minimum droplet size, (d_{jmin}). The minimum droplet size is related to the effective turbulent energy dissipation rate (Lehr et al., 2002; Kolmogorov, 1949; Hinze, 1955; Khadem and Sheibat-Othman, 2019) as:

$$d_{jmin} = d_{jref}\left(\frac{\varepsilon_{eff,j}}{1}\right)^{-0.4} \tag{20}$$

Where $\varepsilon_{eff,j}$ is an effective energy dissipation rate capable of interacting with droplets larger than d_{jmin}. The proportionality constant, d_{jref} (that is d_{jmin} at $\varepsilon_{eff,j} = 1\ m^2/s^3$) is neither dependent on device nor on operating condition. For the rapeseed oil (RO) in water emulsions considered in this work, the values of d_{jref} were set to 450, 100 microns for $j = 1, 2$ respectively for all simulations. For the Group 3 comprising smallest droplets generated by cavitation, $d_{3\min}$ is directly specified based on the experimental data.

The drop breakage rate (k) is formulated as a complex function of energy dissipation rates and droplet diameter (Luo and Svendsen, 1996; Ji et al., 2021):

$$k \quad \alpha \quad \frac{\varepsilon^{1/3}}{d^{2/3}} \quad P(\varepsilon, d) \tag{21}$$

Where $P(\varepsilon, d)$ is a breakage probability. Considering the dependence of diameter on energy dissipation rate and approximating the probability of breakage, in this work, the effective rate of equilibration is approximated as:

$$k_j = k_{jref} \quad \left(\frac{\varepsilon_{eff,j}}{1}\right)^{0.4} \tag{22}$$

Where the proportionality constant, k_{jref} (that is value of k_j at $\varepsilon_{eff,j}$= 1 m^2/s^3), is a function of device design. The values of k_{jref} were obtained for considered three devices by comparing model predictions with the experimental data and are listed in Table 2. The values were not adjusted any further. Eq. (22) represents the equilibrium rate with which the droplet reduces from its initial size to minimum size within a droplet group for a fluidic device. The good agreement observed between the simulated and experimental results provides support for this approximation.

The inter-group breakage rate constants may be estimated by using Eq. (8) following the model of Laakkonen. The values of parameters C_2 and C_3 in Eq. (8) are listed in Table 2 as recommended in (Laakkonen et al., 2006). The value of the parameter C_1 is a system-specific, has a significant influence on simulated results and needs to be obtained from experimental data (Gemello et al., 2019). In this work, we used droplet size distributions obtained for a wide range of energy dissipation rates and found that the dependence of the value of C_1 on energy dissipation rate ($\varepsilon_{eff,j}$) is adequately represented over a wide range of energy dissipation rates (see Figure S5 of supplementary information):

$$C_1 = b_2\left(\frac{\varepsilon_{eff,j}}{1}\right)^{-0.2} \tag{23}$$

The parameter b_2 (that is value of C_1 at $\varepsilon_{eff,j}$= 1 m^2/s^3), depends on the type of fluidic device and does not change with the operating conditions. Please note that though values of C_1 decreases with the effective energy dissipation rate, the breakage rate constant estimated by Eq. (8) always increases with an increase in the effective energy dissipation rate. The values of proportionality constant, b_2, were set for the three devices considered in this work and were not adjusted any further (as listed in Table 2).

For using Eqs. (20), (22) and (23), it is essential to estimate effective energy dissipation rate, $\varepsilon_{eff,j}$. The effective energy dissipation rate will be function of droplet diameter (droplet group, j), flow characteristics of specific device which control distribution of energy dissipation rate within that fluidic device and mean energy dissipation rate ($\bar{\varepsilon}$). The mean energy dissipation rate ($\bar{\varepsilon}$) can be calculated as:

$$\bar{\varepsilon} = \frac{\Delta P \quad q}{\rho \quad V_D} \tag{24}$$

Where ΔP is the pressure drop across the device, q is the flow rate through device, ρ is density and V_D is volume of device. The accuracy of calculated values of mean energy dissipation rates depends on the accuracy of measured pressure drop and flow rate through fluidic devices. The density of fluid and volume of fluidic devices are known. Considering this, the mean energy dissipation rates estimated using Eq. (24) will be within ±5 % which is adequate for the purpose. The values of mean energy dissipation rates for the experiments considered in this work are listed in Table 1. It should however be noted that the effective energy dissipation rate will be different than the mean energy dissipation rate given by Eq. (24). In the presence of surfactants, the minimum droplet diameter will depend on the maximum energy dissipation rate it encounters that can break the particles larger than d_{jmin}. The effective energy dissipation rate therefore will be dependent on the d_{jmin} as well as specific device design in addition to the mean dissipation rate as:

$$\varepsilon_{eff,j} = \alpha_j^D \quad \bar{\varepsilon} \tag{25}$$

Where α_j^D is the ratio of the effective energy dissipation rate to the mean energy dissipation rate for Group j and device D. It therefore has two components. The first one is related to the fluidic device: Every fluidic device considered in this work has a different design and different flow characteristics (Thaker and Ranade, 2022b; Ghanami and Farhadi, 2019b; Springer et al., 2009a). Each device therefore has a different distribution of energy dissipation rates around the mean energy dissipation rates. The ratio of maximum energy dissipation rate to mean energy dissipation rates will be different for each device. The second

Table 2
Model parameters (fixed and adjustable) used with FO, HC, VD (d_{1ref}, d_{2ref}, C_2 and C_3 are 450 μm, 100 μm, 0.04 and 0.01).

S. No.	Fluidic device	ΔP (kPa)	d_{1min}	d_{2min}	d_{3min}	α_j^D			k_{1ref} ($m^{-2}s^{-1}$)	k_{2ref} ($m^{-2}s^{-1}$)	b_2 ($m^{4/3}s^{-3}$)
						α_1	α_2	α_{cav}			
1	Fluidic oscillator (FO)	1.8	110	75	-	60	6	-	1×10^{-3}	1×10^{-6}	9×10^{-4}
		6.4	94	55	-						
		10.6	93	30	-						
2	Helical coil (HC)	96.7	126	4	-	35	80	-	2×10^{-7}	8×10^{-5}	0.0123
		130.5	100	2	-						
		170	100	2	-						
3	Vortex diode (VD)	50	20	>3	3	13	6	20	1×10^{-6}	6×10^{-5}	1×10^{-5}
		150	20	>2.5	2.5						
		250	5	>1.7	1.7						

part is related to the "effective" energy dissipation rate for droplet breakage (Ji et al., 2021). The turbulent flow occurring in the fluidic devices will comprise of wide distribution of length and time scales (Razzaghi and Shahraki, 2016). Only part of these turbulent lengths and time scales will be effective in breaking droplets (Lehr et al., 2002; Chen et al., 2020). Eddies larger than droplets may simply transport the droplets rather than break them. Eddies much smaller than droplet sizes may have a much smaller mean lifetime (and energy) which is not adequate to break the droplet. Thus, only a specific size range of turbulent eddies will be effective in droplet breakage. The parameter, α_j^D, accounts for both these effects, device-specific distribution of energy dissipation rates and droplet size-specific "effective" fraction of energy dissipation and therefore it depends both on the characteristic droplet size of the group as well as the fluidic device. The values of parameter, α_j^D, obtained for the considered devices and system are listed in Table 2.

The model equations, the equations presented in this section (Eqs. 20, 22–25) and the parameters listed in Table 2 allow the solution of model equations provided that the device volume and operating conditions are known so that the mean energy dissipation rate can be estimated using Eq. (24). The accuracy and sensitivity of the simulated results using the simplified drop breakage model are presented in Section S7 of supplementary information. By solving the model equations, the values of d_j and n_j as a function of the number of passes can be calculated. Once the values of d_j and n_j are known, the Sauter mean diameter may be obtained as:

$$d_{32} = \frac{\sum d_j^3 n_j}{\sum d_j^2 n_j} \tag{26}$$

On the first glance, it appears that the presented model has too many parameters. It should however be noted that system specific information and corresponding breakage rates are needed parameters for any breakage models based on MOM or CFD. For the simplified model

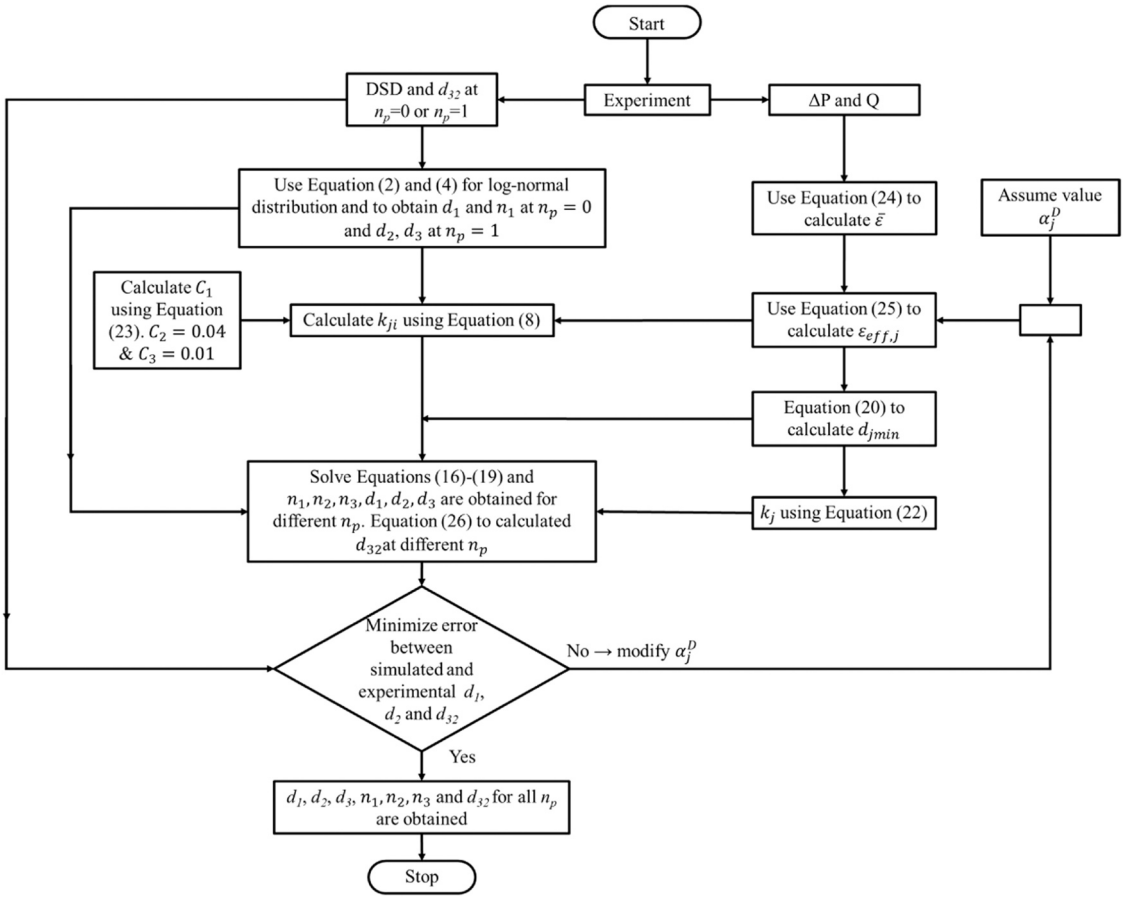

Fig. 5. Flow chart for application of the developed simplified drop breakage model in this work.

presented here, out of the four model parameters α_j^D, d_{jref}, k_{jref} and b_2, three parameters are independent of operating conditions. Since in all the equations in which d_{jref}, k_{jref} and b_2 appears also involve α_j^D, it is possible to treat only α_j^Das an adjustable parameter while setting the d_{jref}, k_{jref} and b_2 to reasonable values. The values of d_{jref}, k_{jref} and b_2 were set to those listed in Table 2 and were not treated like adjustable parameters. The parameters α_j^D, were treated as adjustable parameters and were obtained by minimising the error between the simulated and experimentally obtained d_1, d_2 and d_{32} at different numbers of passes for the devices and operating conditions considered in this work. The overall process followed for obtaining the fitted values of α_j^D is shown schematically in Fig. 5. The values of the parameters α_j^D obtained following this process are listed in Table 2. The application of the model for the emulsions generated with three devices is discussed in the following.

4.2. Emulsions using Fluidic Oscillator (FO)

Droplet size distribution (volume-based, vDSD) measured for 5 % RO in water emulsions produced using FO are shown in Fig. 6. It can be seen that the vDSD is monomodal. The shear rates and energy dissipation rates in FO (Madane and Ranade, 2023) are rather moderate: shear rates are ~10^3 s^{-1} and mean energy dissipation rates are in the range of 10^0 - 10^1 m^2/s^3. These prevailing conditions in FO are not adequate to realise Sauter mean diameter (d_{32}) smaller than 50 μm. Very fine droplets are therefore not formed unlike HC and VD and therefore a mono-modal distribution is observed. The measured vDSD was used to evaluate the application of the simplified droplet breakage model discussed earlier. The values d_1 and d_2 are obtained from the vDSD at n_p=0 and n_p =1 (refer to Fig. 6). The model was used to simulate the variation of d_1 and d_2, with the number of passes as shown in Fig. 7a. The corresponding profiles of the number of droplets in groups 1 and 2 are shown in Fig. 7b. The values of α_j^D for FO was found to be 1 for both the droplet groups (see Table 2). It can be seen that the simplified breakage model is able to describe the experimental data reasonably well.

The developed model was then used to simulate the influence of pressure drop across FO on resulting drop breakage. As the flow rate increased, the mean effective energy dissipation rate increased leading to a greater reduction in droplet sizes (d_{32}) as shown in Fig. 8. For example, an increase in flow rate from 1 LPM to 3 LPM through FO led to almost 100 % reduction in the Sauter mean diameters obtained after 200 passes (d_{32} reduced from 98 to 51 microns). Increased flow rate in FO increases jet oscillation frequency (Madane and Ranade, 2023). The enhanced jet oscillations increase corresponding shear rates and cause enhanced droplet breakage. The variation of Sauter mean diameter with respect to the number of passes at three flow rates through FO is shown in Fig. 8. The continuous lines shown in Fig. 8 represent the values of Sauter mean diameter calculated from the simplified breakage model (from simulated values of d_1, d_2, n_1 and n_2). It can be seen from Fig. 8 that the simplified droplet breakage model was able to capture the influence of flow rate and number of passes through FO quite well. The model was then used for the other two fluidic devices having much higher energy dissipation rates than FO.

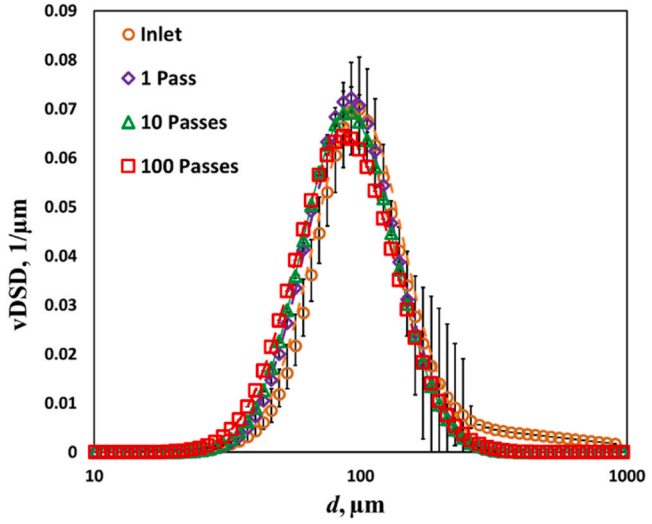

Fig. 6. Fluidic oscillator (ΔP = 1.8 kPa) vDSD obtained using FBRM (symbols) and corresponding predictions of vDSD with the log-normal fit (lines) for 5 % rapeseed oil in the emulsion. (1 pass: μ = 4.686; σ = 0.401; 10 passes: μ = 4.654; σ = 0.398; 100 passes: μ = 4.651; σ = 0.427). (Dashed lines represent the simulated results and the symbols of the same colour of the lines denote corresponding experimental data).

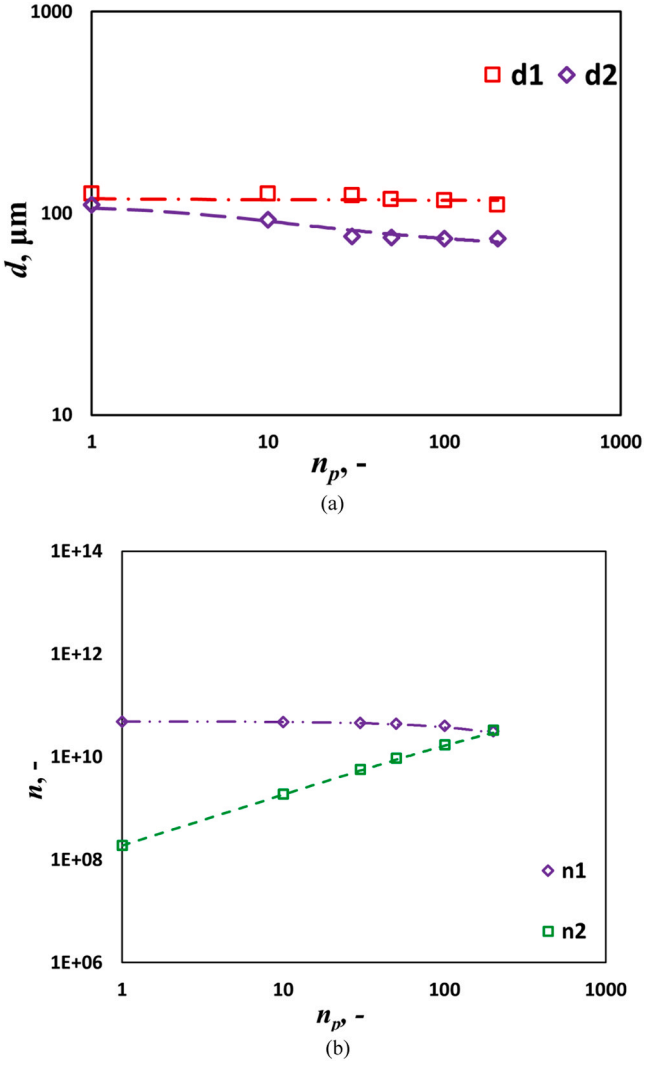

Fig. 7. Comparison of (a) diameter variations; (b) number of drops per unit volume (n) obtained from experiments and breakage model for α_0 = 0.05 RO in FO (ΔP = 1.8 kPa). Parameters of the simplified breakage model are listed in Table S4 of SI. (Dashed lines represent the simulated results and the symbols of the same colour of the lines denote corresponding experimental data).

4.3. Emulsions using Helical Coil (HC)

Emulsions produced with HC exhibited bimodal droplet size distributions. The experimentally measured vDSD for three different numbers of passes through HC are shown in Fig. 9. The bi-modal nature of DSD is evident from Fig. 9. The formation of this bimodal vDSD is attributed to

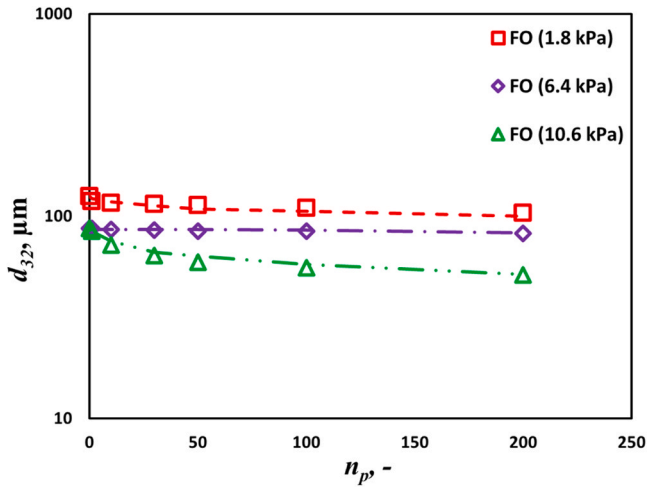

Fig. 8. Comparison of experimental and simulated results d_{32} of FO at different pressure drops (Dashed lines represent the simulated results and the symbols of the same colour of the lines denote corresponding experimental data).

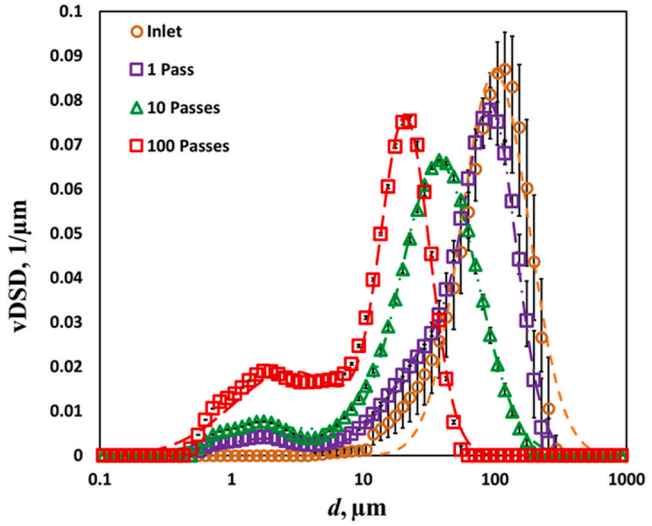

Fig. 9. Helical coil (ΔP = 96.7 kPa) vDSD obtained using MasterSizer and corresponding predictions of vDSD with the log-normal fit for 5 % rapeseed oil in the emulsion at ΔP = 96.7 kPa (Log-normal fit for 1 pass: $\mu_1 = 4.320$; $\sigma_1 = 0.875$; $\mu_2 = 4.743$; $\sigma_2 = 0.443$) (Log-normal fit for 10 passes: $\mu_1 = 4.078$; $\sigma_1 = 0.669$; $\mu_2 = 2.096$; $\sigma_2 = 1.083$) (Log-normal fit for 100 passes: $\mu_1 = 2.108$; $\sigma_1 = 1.027$; $\mu_2 = 3.226$; $\sigma_2 = 0.428$). Dashed lines represent the simulated results and the symbols of the same colour of the lines denote corresponding experimental data.

the physical phenomena occurring inside the HC. When the pre-emulsion flows through the HC, the drops which are near the HC wall experience intense turbulence shear ($\varepsilon \sim 10^2$ m^2/s^3). In contrast, the droplets traversing the center of the coil experience comparatively lower shear stress. These widely different shear rates and local energy dissipation rates within HC lead to the observed bi-modal nature of vDSD. The secondary flows (Dean's vortices) generated in HC (Springer et al., 2009b; Moll et al., 2002) further complicate the matter by causing the mixing of droplets passing through different zones. This intermixing leads to wider droplet size distributions. The droplet sizes observed with HC are much smaller (almost by an order of magnitude) than those observed with FO. The number of passes through HC also has a significant impact on the reduction in droplet sizes compared to that observed in the case of FO. The Sauter mean diameter was reduced from 9 µm to 3 µm for $n_p = 200$ when the flow rate was increased from 1 to 3 LPM. The simplified droplet breakage model was applied to the emulsions produced with HC.

As an illustration of the application of the simplified droplet breakage model, a case of emulsions produced with HC operated at ΔP = 96.7 kPa is considered here. The model parameters were obtained as discussed earlier. For HC, mean energy dissipation rates are higher compared to FO which leads to significantly smaller droplet sizes in HC. The variation of d_1 and d_2 obtained from the simulated result of the model is shown in Fig. 10a. The corresponding profiles of the number of droplets in Groups 1 and 2 are shown in Fig. 10b. It can be seen from Fig. 10 that the experimental results can be well described by the simplified model. The fitted values of α_j^D for HC were found to be 26 and 75 for $j = 1$ and 2 respectively (see Table 2). Unlike FO, there is a considerable reduction in drop diameter from d_1 to $d_{1\,min}$ as the number of passes increases. This is primarily because of exposure to larger values of ε_1 ($\sim 10^4$ m^2/s^3) for HC at 96.7 kPa. The diameter reduction for Group 2 droplets, d_2 to $d_{2\,min}$ is rather small compared to that observed in the case of d_1. This is because of the already small size of droplets of Group 2.

The simplified breakage model was then used to simulate drop breakage at different operating conditions (higher flow rate and

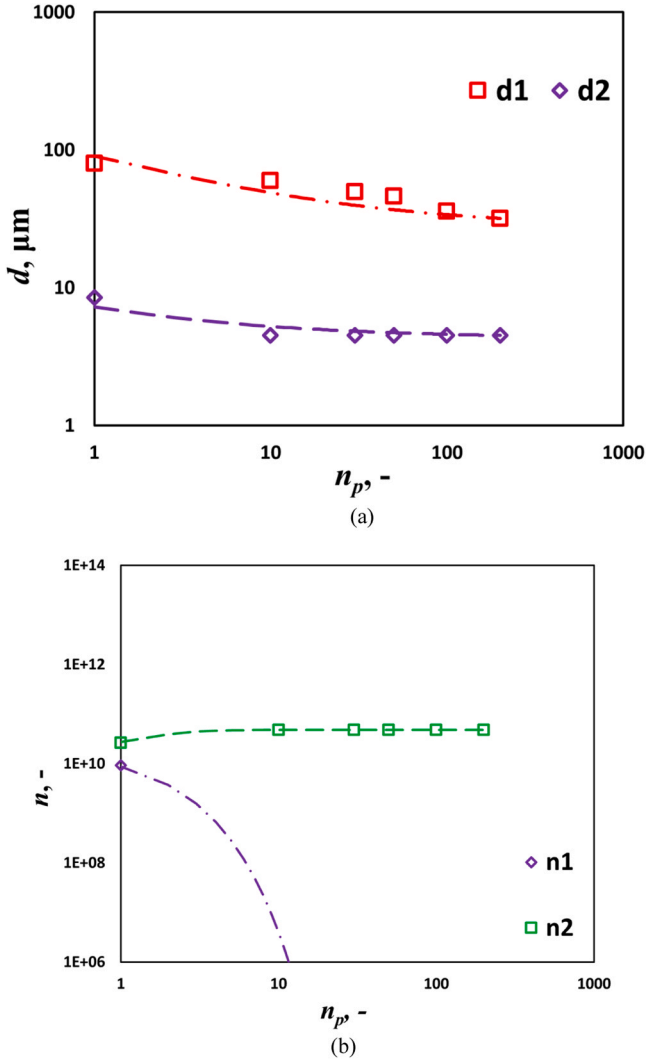

Fig. 10. Comparison of (a) diameter variations; (b) number of drops per unit volume (n) obtained from experiments and breakage model for $\alpha_0 = 0.05$ RO in HC (ΔP = 96.7 kPa). Parameters of the simplified breakage model are listed in Table S4 of SI. Dashed lines represent the simulated results and the symbols of the same colour of the lines denote corresponding experimental data.

therefore higher pressure drop). The comparison of simulated variation of Sauter mean diameter as a function of the number of passes and pressure drop across HC is shown in Fig. 11. The Sauter mean diameter was found to decrease significantly with an increase in the number of passes in the initial phase. However, as the number of passes increases beyond 50, the further reduction in the Sauter mean diameter with the number of passes is rather slow. Considering the high prevailing effective energy dissipation rates in HC, this is likely to be because of the significant breakage of Group 1 particles with few initial passes. It can be seen from Fig. 10b that the number of droplets of Group 1 is reduced by orders of magnitude before 3 passes because of which the number of droplets of Group 2 appears to be constant from the beginning. It can be seen from Fig. 11 that the simplified model captured the experimental data quite well. In both the devices discussed so far, there was no cavitation and therefore the droplets belonging to the smallest group, Group 3 were absent. The model was then evaluated by simulating emulsions using a cavitation device (VD).

4.4. Emulsion using Vortex-based Cavitation Device (VD)

The vortex-based cavitation device (VD) was shown to produce a bimodal distribution and a significant reduction in droplet sizes even with a single pass (Thaker and Ranade, 2021a). As the number of passes increases, the droplet size decreases further (Thaker and Ranade, 2022b). In a single pass-through VD, only a fraction of the droplets of the emulsion may pass through the cavitating core and encounter collapsing cavities. The other fraction of droplets may not encounter collapsing cavities and get broken because of prevailing turbulence and shear in the VD besides the cavitating core region. The droplets not encountering collapsing cavities are broken down into droplets of $\sim 10^1$μm. There is a finite fraction of droplets encountering collapsing cavities which are broken down to $\sim 10^0$μm (see measured droplet size distribution shown in Fig. 12). These two different droplet mechanisms lead to the bimodal nature of the resulting DSD. As the n_p increases, there is a more and more chance that droplets encounter collapsing cavities and therefore eventually bimodal nature of DSD vanishes at 100 passes and beyond as seen in Fig. 12. The vDSD of pre-emulsion and 1 pass is utilized in the simplified drop breakage model and the steps mentioned in Section 4.1 are followed.

The simplified breakage model is applied to the data from VD. Unlike the previous two devices, Group 3 droplets comprising small droplets

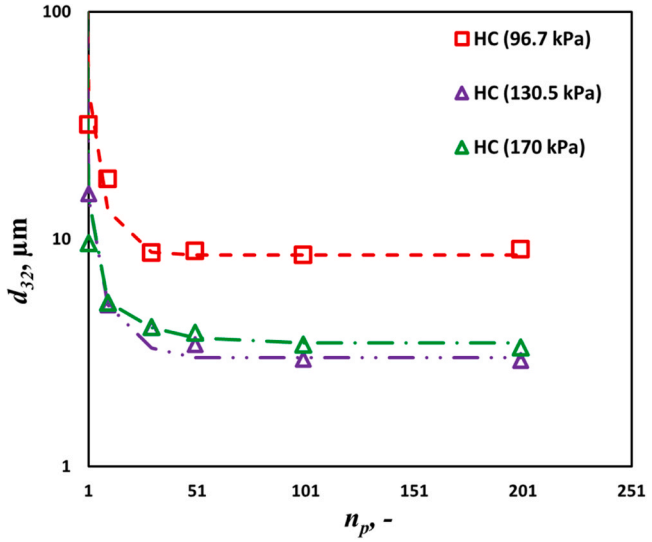

Fig. 11. Comparison of experimental and simulated results d_{32} of HC at different pressure drops Dashed lines represent the simulated results and the symbols of the same colour of the lines denote corresponding experimental data.

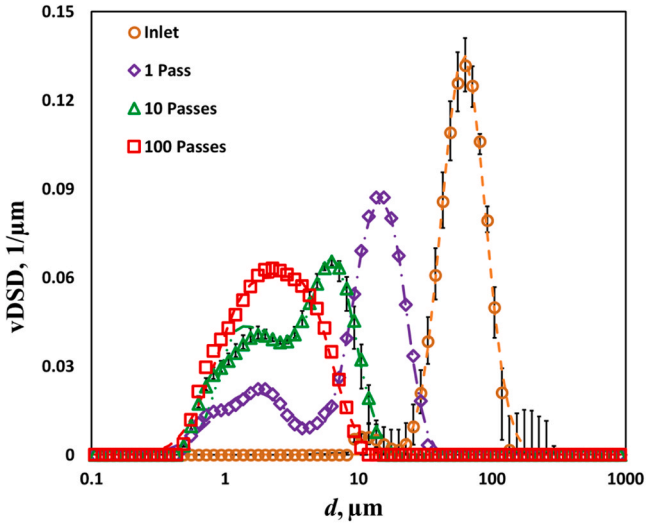

Fig. 12. Vortex diode (ΔP = 250 kPa) vDSD obtained using MasterSizer and corresponding predictions of vDSD with the log-normal fit for 5 % rapeseed oil in the emulsion at ΔP = 250 kPa (Log-normal fit for 1 pass: μ_1 = 3.053; σ_1= 0.256; μ_2 = 0.959; σ_2= 0.981; μ_3 = 2.697; σ_3= 0.382) (Log-normal fit for 10 passes: μ_1 = 2.026; σ_1= 0.386; μ_2 = 0.163; σ_2= 0.250; μ_3 = 0.988; σ_3= 0.586) (Log-normal fit for 100 passes: μ_1 = 1.165; σ_1= 0.607; μ_2 = 0.828; σ_2= 0.603; μ_3 = 1.650; σ_3= 0.433). Dashed lines represent the simulated results and the symbols of the same colour of the lines denote corresponding experimental data.

caused by collapsing cavities are included in the model. In VD, due to extremely high energy dissipation rates per unit mass caused by collapsing cavities (10^7 - 10^8 m^2/s^3), the droplets of Group 3 have a diameter equal to $d_{3\,min}$. As the number of passes increases beyond 100, effectively mono-modal distribution forms (from Fig. 12). The simulated results of diameter variation and number of drops with the passes for the case of ΔP = 250 kPa for two values of oil volume fraction (5 and 15 %) are shown in Fig. 13. The corresponding model parameters are listed in Table 2. It can be seen that the simulated results agree well with the experimental data. Exposure to such high energy dissipation rates cause intense droplet breakage in first few passes through the cavitation device. Therefore, no significant breakage occurs after 10 passes. This leads to much flatter profile of droplet diameters with number of passes compared to the other two devices having orders of magnitude lower energy dissipation (refer Table S5 of supplementary information). The values of $d_{1\,min}$ and $d_{2\,min}$ for the case of VD are lower than those observed for HC and FO. The model was then applied to two other operating conditions of VD. The simulated results of Sauter mean diameter are compared with the experimental data in Fig. 14. It can be seen that, like HC, the Sauter mean diameter decreases sharply with the initial few passes and then decreases gradually. In the case of VD, the phase of rapid reduction in Sauter mean diameter lasts only up to 10 passes unlike in HC where it lasts up to nearly 50 passes. It can be seen that the simplified model can capture the influence of pressure drop (flow rate) as well as the number of passes on Sauter mean diameter quite well.

It will be instructive to compare the obtained drop breakage efficiency (η) for the three emulsion-producing devices as a function of energy consumption (Thaker and Ranade, 2022b). The drop breakage efficiency (η) and energy consumption per unit mass of emulsion (E) can be obtained from:

$$\eta = \frac{6\alpha_O\sigma}{\Delta P n_p}\left[\left(\frac{1}{d_{32}}\right)_{n_p} - \frac{1}{d_{320}}\right] \tag{27}$$

$$E = \frac{\Delta P n_p}{\rho_m} \tag{28}$$

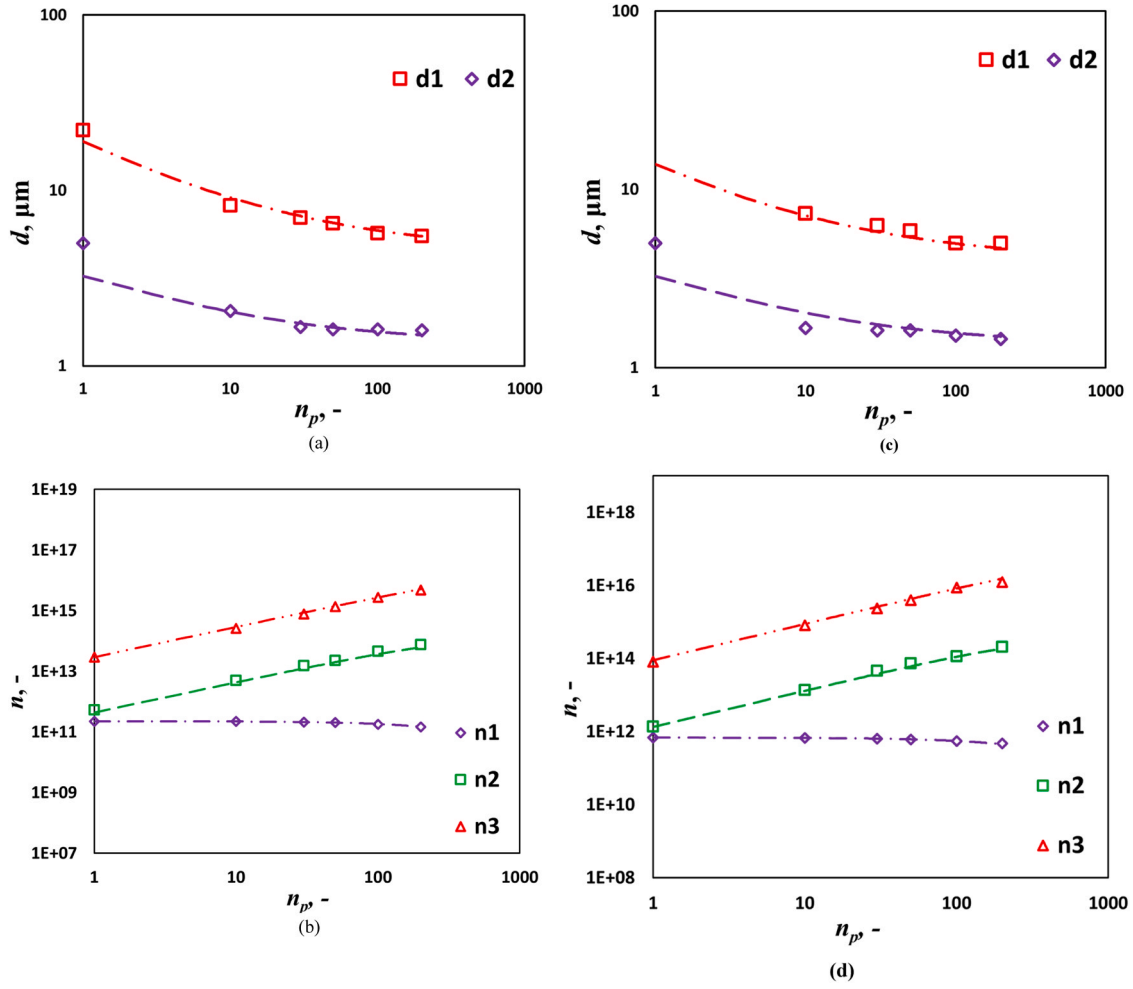

Fig. 13. Comparison of simulated and experimental results (a) diameter variations; (b) number of drops per unit volume (n) obtained from experiments and drop breakage model for $\alpha_0 = 0.05$ for VD ($\Delta P = 250$ kPa); and (c) diameter variations for $\alpha_0 = 0.15$ RO (d) number of drops per unit volume (n) for $\alpha_0 = 0.15$ RO. Parameters of the simplified breakage model are listed in Table S4 of SI. Dashed lines represent the simulated results and the symbols of the same colour of the lines denote corresponding experimental data.

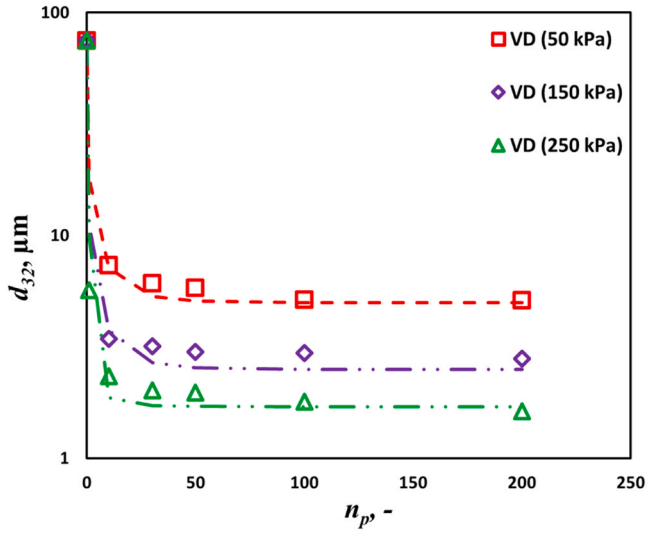

Fig. 14. Comparison of experimental and simulated results d_{32} of VD at different pressure drops. Dashed lines represent the simulated results and the symbols of the same colour of the lines denote corresponding experimental data.

Where, d_{320} is Sauter mean diameter of pre-emulsion, $(d_{32})_{n_p}$ is Sauter mean diameter for different passes, α_O, σ, ΔP, n_p and ρ_m are the volume fraction of oil, interfacial tension (N/m), pressure drop (Pa), number of passes and density of emulsion (kg/m^3), respectively. The results of η obtained for all three fluidic devices at typical operating conditions are shown in Fig. 15. It can be seen that breakage efficiency obtained from the simplified model captured key trends for all three devices correctly. It can be seen from Fig. 15 that the lowest drop breakage efficiency is observed in FO which is one order of magnitude lower than that obtained with HC. VD exhibits the highest drop breakage efficiency. Considering the operating ranges, FO is a preferred choice for low (< 20 J/kg) energy consumption, HC for the middle range (20 – 100 J/kg) and VD for the higher (> 100 J/kg) range of energy consumption.

The simulated results show good agreement with the experimental results for the d_{32} of all the fluidic devices and operating conditions used in this work using adjustable parameter, α_j^D. The value of this parameter, α_j^D, indicating the ratio of effective energy dissipation rate to mean energy dissipation rate may in principle be obtained by carrying out detailed turbulent multiphase flow simulations (which are outside the scope of this work). The simplified droplet breakage model can therefore be used for evaluating different fluidic devices and operating conditions. The developed approach and the model will be useful for designing appropriate devices and operating conditions to obtain emulsions of the desired DSD or Sauter mean diameter.

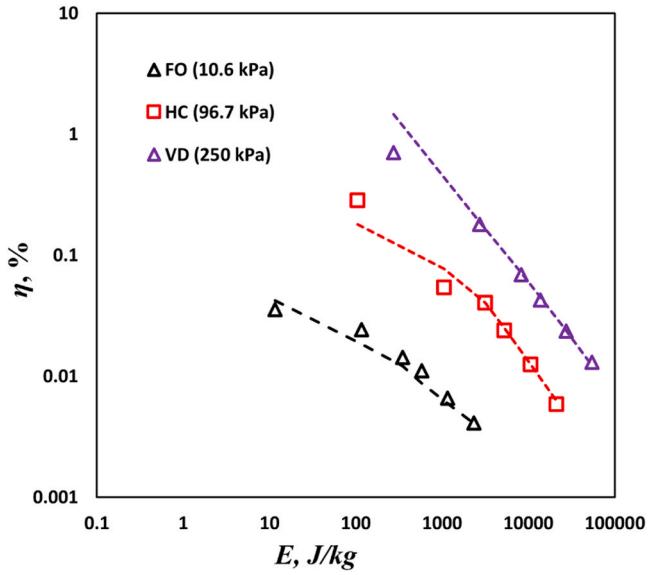

Fig. 15. Variation of breakage efficiency (η) with energy consumption per unit mass of emulsion. Dashed lines represent the simulated results and the symbols of the same colour of the lines denote corresponding experimental data.

5. Conclusions

We developed a simplified drop breakage model and have shown its applicability to simulate the variation of droplet diameters with the number of passes through three different fluidic devices namely, fluidic oscillator, helical coil, and vortex-based cavitation device. The simplified model was shown to describe the experimental data over a wide range of operating conditions spanning four orders of mean energy dissipation rates (10^0 to 10^4 m^2/s^3). The key findings of the present work are summarized in the following:

- Among the three devices investigated here, the vortex-based cavitation device was found to generate emulsion with the smallest droplets (1–2 μm). Helical coil also produced reasonably small droplets even in the absence of cavitation (3–8 μm). The fluidic oscillator with the lowest energy dissipation rates generated emulsions with droplets in the range of 40–100 μm.
- The developed simplified breakage model and the developed relationships of minimum diameter and breakage rate constants with respect to effective energy dissipation rates were found to describe the variation of Sauter mean diameter with respect to the number of passes quite well.
- The simplified breakage model was able to capture the influence of operating conditions and different devices on droplet breakage efficiency adequately.
- Cavitation device, VD exhibits the highest breakage efficiency and is a preferred choice for producing fine emulsions when energy consumption per unit mass of more than 100 J/kg can be afforded. For low energy consumption applications (less than 20 J/kg), FO is the preferred choice. At the intermediate range, HC is a preferred choice. If emulsions with a Sauter mean diameter of ~1 micron are desired, a cavitation device is the best.

The developed approach and the presented model will be useful for practising engineers in the selection of appropriate fluidic devices and operating conditions.

CRediT authorship contribution statement

Deepak K. Pandey: Data curation, Formal analysis, Investigation, Methodology, Validation, Writing – original draft. **Vivek V. Ranade:** Conceptualization, Funding acquisition, Methodology, Project administration, Supervision, Writing – review & editing. **Abhijeet H. Thaker:** Data curation, Formal analysis, Investigation.

Declaration of Competing Interest

The authors declare that they have no known competing financial interests or personal relationships that could have appeared to influence the work reported in this paper

Data availability

The data that support the findings of this study are available from the corresponding author upon reasonable request.

Acknowledgement

The authors greatly acknowledge financial support from the Science Foundation Ireland (SFI Project ID: 20/FFP-A/ 8518).

Appendix A. Supporting information

Supplementary data associated with this article can be found in the online version at doi:10.1016/j.cherd.2024.04.038.

References

Alopaeus, V., Koskinen, J., I. Keskinen, K., Majander, J., 2002a. Simulation of the population balances for liquid-liquid systems in a nonideal stirred tank. Part 2-parameter fitting and the use of the multiblock model for dense dispersions. Chem. Eng. Sci. 57, 1815–1825. https://doi.org/10.1016/S0009-2509(02)00067-2.

Alopaeus, V., Koskinen, J., I. Keskinen, K., Majander, J., 2002b. Simulation of the population balances for liquid–liquid systems in a nonideal stirred tank. Part 2—parameter fitting and the use of the multiblock model for dense dispersions. Chem. Eng. Sci. 57, 1815–1825. https://doi.org/10.1016/S0009-2509(02)00067-2.

Andersson, B., Andersson, R., Håkansson, L., Mortensen, M., Sudiyo, R., Van, B., Frontmatter, W., 2011. Computational Fluid Dynamics for Engineers. Cambridge University Press, Cambridge. https://doi.org/10.1017/CBO9781139093590.

Andersson, R., Andersson, B., 2006. Modeling the breakup of fluid particles in turbulent flows. AIChE J. 52, 2031–2038. https://doi.org/10.1002/AIC.10832.

Ashokkumar, M., Rink, R., Shestakov, S., Tee, K., Federation, R., 2011. Hydrodynamic cavitation - an alternative to ultrasonic food processing. Tech. Acoust. 9, 1–10.

Becker, J., Puel, F., Chevalier, Y., Sheibat-Othman, N., 2013. Monitoring Silicone Oil Droplets During Emulsification in Stirred Vessel: Effect of Dispersed Phase Concentration and Viscosity. Can. J. Chem. Eng. 92 https://doi.org/10.1002/cjce.21885.

Carpenter, J., George, S., Saharan, V.K., 2017. Low pressure hydrodynamic cavitating device for producing highly stable oil in water emulsion: Effect of geometry and cavitation number. Chem. Eng. Process. 116, 97–104. https://doi.org/10.1016/J.CEP.2017.02.013.

Chen, Y., Ding, J., Weng, P., Yang, X., Wu, W., 2020. On the breakup of Taylor length scale size bubbles and droplets in turbulent dispersions. Chem. Eng. J. 386 https://doi.org/10.1016/j.cej.2019.05.187.

Coulaloglou, C.A., Tavlarides, L.L., 1977a. Description of interaction processes in agitated liquid-liquid dispersions. Chem. Eng. Sci. 32, 1289–1297. https://doi.org/10.1016/0009-2509(77)85023-9.

Coulaloglou, C.A., Tavlarides, L.L., 1977b. Description of interaction processes in agitated liquid-liquid dispersions. Chem. Eng. Sci. 32, 1289–1297. https://doi.org/10.1016/0009-2509(77)85023-9.

Dillon, I.J., Campbell, K.M., Mantripragada, S., 2020. Coiled Tube Émuls. Methods 20200129443.

Fesenko, A., Yevsiukova, F., Basova, Y., Ivanova, M., Ivanov, V., 2018. Prospects of using hydrodynamic cavitation for enhancement of efficiency of fluid working medium preparation technologies. Period. Polytech. Mech. Eng. 62, 269–276. https://doi.org/10.3311/PPME.11877.

Gemello, L., Plais, C., Augier, F., Marchisio, D.L., 2019. Population balance modelling of bubble columns under the heterogeneous flow regime. Chem. Eng. J. 372, 590–604. https://doi.org/10.1016/j.cej.2019.04.109.

Ghanami, S., Farhadi, M., 2019a. Fluidic Oscillators' Applications, Structures and Mechanisms-A review. Nano Micro Scales 7, 9–27. https://doi.org/10.22111/tpnms.2018.25051.1153.

Ghanami, S., Farhadi, M., 2019b. Fluidic oscillators' applications, structures and mechanisms-a review. Nano Micro Scales 7, 9–27. https://doi.org/10.22111/tpnms.2018.25051.1153.

Gohtani, S., Prasert, W., 2014. Nano-Emulsions; Emulsification Using Low Energy Methods. Jpn. J. Food Eng. 15, 119–130.

Groeneweg, F., van Dieren, F., Agterof, W.G.M., 1994. Droplet break-up in a stirred water-in-oil emulsion in the presence of emulsifiers. Colloids Surf. A Physicochem Eng. Asp. 91, 207–214. https://doi.org/10.1016/0927-7757(94)02913-X.
Guo, K., Wang, T., Liu, Y., Wang, J., 2017. CFD-PBM simulations of a bubble column with different liquid properties. Chem. Eng. J. 329, 116–127. https://doi.org/10.1016/J.CEJ.2017.04.071.
Gupta, A., Eral, H.Burak, Hatton, T.A., Doyle, P.S., 2016. Nanoemulsions: formation, properties and applications. Soft Matter 12, 2826. https://doi.org/10.1039/c5sm02958a.
Hanotu, J., Bandulasena, H.C.H., Chiu, T.Y., Zimmerman, W.B., 2013. Oil emulsion separation with fluidic oscillator generated microbubbles. Int. J. Multiph. Flow. 56, 119–125. https://doi.org/10.1016/j.ijmultiphaseflow.2013.05.012.
Han, L., Luo, H., Liu, Y., 2011. A theoretical model for droplet breakup in turbulent dispersions. Chem. Eng. Sci. 66, 766–776. https://doi.org/10.1016/J.CES.2010.11.041.
Hinze, J.O., 1955. Fundamentals of the hydrodynamic mechanism of splitting in dispersion processes. AIChE J. 1, 289–295.
Ji, Y., Bellettre, J., Montillet, A., Massoli, P., 2021. Experimental investigation on single drop breakage in two-stream impinging microchannels. Exp. Fluids 62. https://doi.org/10.1007/s00348-020-03124-0.
Kamp, J., Nachtigall, S., Maaß, S., Kraume, M., 2012. Modelling of coalescence in turbulent liquid/liquid dispersions considering droplet charge. Czas. Tech. Mech. 109.
Karunaratne, D.N., Pamunuwa, G., Ranatunga, U., 2017. Introductory Chapter: Microemulsions. In: Properties and Uses of Microemulsions. InTech. https://doi.org/10.5772/intechopen.68823.
Khadem, B., Sheibat-Othman, N., 2019. Theoretical and Experimental Investigations of Double Emulsion Preparation by Ultrasonication. Ind. Eng. Chem. Res 58, 8220–8230. https://doi.org/10.1021/acs.iecr.9b00556.
Khalil, A., Puel, F., Chevalier, Y., Galvan, J.M., Rivoire, A., Klein, J.P., 2010. Study of droplet size distribution during an emulsification process using in situ video probe coupled with an automatic image analysis. Chem. Eng. J. 165, 946–957. https://doi.org/10.1016/J.CEJ.2010.10.031.
Kolmogorov, A., 1949. On the breakage of drops in a turbulent flow. Dokl. Akad. Navk. SSSR 66, 825–828. ⟨https://cir.nii.ac.jp/crid/1573668925359849216.bib?lang=en⟩ (accessed February 3, 2024).
Konno, M., Matsunaga, Y., Arai, K., Saito, S., 1980. Simulation model for breakup process in an agitated tank. J. Chem. Eng. Jpn. 13, 67–73. https://doi.org/10.1252/JCEJ.13.67.
M. Laakkonen, V. Alopaeus, J. Aittamaa, Validation of bubble breakage, coalescence and mass transfer models for gas-liquid dispersion in agitated vessel, in: Chem Eng Sci, 2006: pp. 218–228. https://doi.org/10.1016/j.ces.2004.11.066.
Laakkonen, M., Moilanen, P., Alopaeus, V., Aittamaa, J., 2007. Modelling local bubble size distributions in agitated vessels. Chem. Eng. Sci. 62, 721–740. https://doi.org/10.1016/j.ces.2006.10.006.
Lasheras, J.C., Eastwood, C., Martínez-Bazán, C., Montaes, J.L., 2002. A review of statistical models for the break-up an immiscible fluid immersed into a fully developed turbulent flow. Int. J. Multiph. Flow. 28, 247–278. https://doi.org/10.1016/S0301-9322(01)00046-5.
Lehr, F., Millies, M., Mewes, D., 2002. Bubble-size distributions and flow fields in bubble columns. AIChE J. 48, 2426–2443. https://doi.org/10.1002/aic.690481103.
Liao, Y., Lucas, D., 2009. A literature review of theoretical models for drop and bubble breakup in turbulent dispersions. Chem. Eng. Sci. 64, 3389–3406. https://doi.org/10.1016/j.ces.2009.04.026.
Li, J., Barrow, D.A., 2017. A new droplet-forming fluidic junction for the generation of highly compartmentalised capsules. Lab Chip 17, 2873–2881. https://doi.org/10.1039/c7lc00618g.
Li, Y., Xiang, D., 2019. Stability of oil-in-water emulsions performed by ultrasound power or high-pressure homogenization. PLoS One 14, e0213189. https://doi.org/10.1371/JOURNAL.PONE.0213189.
Luo, H., Svendsen, H.F., 1996. Theoretical model for drop and bubble breakup in turbulent dispersions. AIChE J. 42, 1225–1233. https://doi.org/10.1002/AIC.690420505.
Maaß, S., Kraume, M., 2012a. Determination of breakage rates using single drop experiments. Chem. Eng. Sci. 70, 146–164. https://doi.org/10.1016/j.ces.2011.08.027.
Maaß, S., Kraume, M., 2012b. Determination of breakage rates using single drop experiments. Chem. Eng. Sci. 70, 146–164. https://doi.org/10.1016/J.CES.2011.08.027.
Madane, K., Khalde, C., Pandit, A., Ranade, V.V., 2023. Flow physics of planar bistable fluidic oscillator with backflow limbs. AIChE J. 69 https://doi.org/10.1002/AIC.17621.
Madane, K., Ranade, V.V., 2022. Anti-solvent crystallization: Particle size distribution with different devices. Chem. Eng. J. 446, 137235 https://doi.org/10.1016/J.CEJ.2022.137235.
Madane, K., Ranade, V., 2023. Jet oscillations and mixing in fluidic oscillators: influence of geometric configuration and scale. Ind. Eng. Chem. Res. https://doi.org/10.1021/acs.iecr.3c02077.
Maindarkar, S.N., Dubbelboer, A., Meuldijk, J., Hoogland, H., Henson, M.A., 2014. Prediction of emulsion drop size distributions in colloid mills. Chem. Eng. Sci. 118, 114–125. https://doi.org/10.1016/j.ces.2014.07.032.
Marchisio, D.L., Di Torino, P., Fox, R.O., 2013. Computational Models for Polydisperse Particulate and Multiphase Systems. Cambridge University Press, Cambridge. https://doi.org/10.1017/CBO9781139016599.
Matiazzo, T., Decker, R.K., Bastos, J.C.S.C., Silva, M.K., Meier, H.F., 2020. Investigation of breakup and coalescence models for churn-turbulent gas-liquid bubble columns. J. Appl. Fluid Mech. 13, 737–751. https://doi.org/10.29252/jafm.13.02.30310.
Moilanen, P., Laakkonen, M., Visuri, O., Alopaeus, V., Aittamaa, J., 2008. Modelling mass transfer in an aerated 0.2 m3 vessel agitated by Rushton, Phasejet and Combijet impellers. Chem. Eng. J. 142, 95–108. https://doi.org/10.1016/J.CEJ.2008.01.033.
Moll, R., Moulin, P., Veyret, D., Charbit, F., 2002. Numerical simulation of Dean vortices: fluid trajectories. J. Memb. Sci. 197, 157–172. https://doi.org/10.1016/S0376-7388(01)00606-8.
Nauha, E.K., Kálal, Z., Ali, J.M., Alopaeus, V., 2018. Compartmental modeling of large stirred tank bioreactors with high gas volume fractions. Chem. Eng. J. 334, 2319–2334. https://doi.org/10.1016/J.CEJ.2017.11.182.
O'Sullivan, J., Murray, B., Flynn, C., Norton, I., 2015. Comparison of batch and continuous ultrasonic emulsification processes. J. Food Eng. 167, 114–121. https://doi.org/10.1016/J.JFOODENG.2015.05.001.
D.K. Pandey, A.H. Thaker, V.V. Ranade, A simplified drop breakage model for fluidic devices with and without hydrodynamic cavitation, in: ChemEngDay UK 2023, 2023.
Pandit, A.V., Ranade, V.V., 2016. Chord length distribution to particle size distribution. AIChE J. 62, 4215–4228. https://doi.org/10.1002/aic.15338.
Pandit, A.V., Sarvothaman, V.P., Ranade, V.V., 2021. Estimation of chemical and physical effects of cavitation by analysis of cavitating single bubble dynamics. Ultrason Sonochem. 77 https://doi.org/10.1016/j.ultsonch.2021.105677.
Parthasarathy, S., Siah Ying, T., Manickam, S., 2013. Generation and optimization of palm oil-based oil-in-water (O/W) submicron-emulsions and encapsulation of curcumin using a liquid whistle hydrodynamic cavitation reactor (LWHCR). Ind. Eng. Chem. Res 52. https://doi.org/10.1021/ie4008858.
Perrier-Cornet, J.M., Marie, P., Gervais, P., 2005. Comparison of emulsification efficiency of protein-stabilized oil-in-water emulsions using jet, high pressure and colloid mill homogenization. J. Food Eng. 66, 211–217. https://doi.org/10.1016/J.JFOODENG.2004.03.008.
Petitti, M., Nasuti, A., Marchisio, D.L., Vanni, M., Baldi, G., Mancini, N., Podenzani, F., 2010. Bubble size distribution modeling in stirred gas-liquid reactors with QMOM augmented by a new correction algorithm. AIChE J. 56, 36–53. https://doi.org/10.1002/aic.12003.
Petitti, M., Vanni, M., Marchisio, D.L., Buffo, A., Podenzani, F., 2013. Simulation of coalescence, break-up and mass transfer in a gas-liquid stirred tank with CQMOM. Chem. Eng. J. 228, 1182–1194. https://doi.org/10.1016/J.CEJ.2013.05.047.
Ramisetty, K.A., Pandit, A.B., Gogate, P.R., 2014. Novel approach of producing oil in water emulsion using hydrodynamic cavitation reactor. Ind. Eng. Chem. Res 53, 16508–16515. https://doi.org/10.1021/ie502753d.
Ranade, V.V., 2022. Modeling of hydrodynamic cavitation reactors: reflections on present status and path forward. ACS Eng. Au. https://doi.org/10.1021/acsengineeringau.2c00025.
Ranade, V.V., Utikar, R.P., 2022. Multiphase Flows for Process Industries: Fundamentals and Applications. John Wiley & Sons. ⟨https://books.google.ie/books?id=kCZnEAAAQBAJ⟩ (accessed January 28, 2024).
Razzaghi, K., Shahraki, F., 2016. Theoretical model for multiple breakup of fluid particles in turbulent flow field. AIChE J. 62, 4508–4525. https://doi.org/10.1002/aic.15314.
Servant, G., Laborde, J.L., Hita, A., Caltagirone, J.P., Gérard, A., 2001. Spatio-temporal dynamics of cavitation bubble clouds in a low frequency reactor: comparison between theoretical and experimental results. Ultrason Sonochem. 8, 163–174. https://doi.org/10.1016/S1350-4177(01)00074-8.
Simpson, A., Ranade, V.V., 2019. Flow characteristics of vortex based cavitation devices computational investigation on influence of operating parameters and scale. AIChE J. 65 https://doi.org/10.1002/aic.16675.
Solsvik, J., Jakobsen, H.A., 2016. Development of fluid particle breakup and coalescence closure models for the complete energy spectrum of isotropic turbulence. Ind. Eng. Chem. Res 55, 1449–1460. https://doi.org/10.1021/acs.iecr.5b04077.
Solsvik, J., Skjervold, V.T., Han, L., Luo, H., Jakobsen, H.A., 2016. A theoretical study on drop breakup modeling in turbulent flows: the inertial subrange versus the entire spectrum of isotropic turbulence. Chem. Eng. Sci. 149, 249–265. https://doi.org/10.1016/J.CES.2016.04.037.
Solsvik, J., Tangen, S., Jakobsen, H.A., 2013. On the constitutive equations for fluid particle breakage. Rev. Chem. Eng. 29, 241–356.
Springer, F., Carretier, E., Veyret, D., Moulin, P., 2009a. Developing lengths in woven and helical tubes with dean vortices flows. Eng. Appl. Comput. Fluid Mech. 3, 123–134. https://doi.org/10.1080/19942060.2009.11015259.
Springer, F., Carretier, E., Veyret, D., Moulin, P., 2009b. Developing lengths in woven and helical tubes with dean vortices flows. Eng. Appl. Comput. Fluid Mech. 3, 123–134. https://doi.org/10.1080/19942060.2009.11015259.
Tang, S.Y., Shridharan, P., Sivakumar, M., 2013. Impact of process parameters in the generation of novel aspirin nanoemulsions–comparative studies between ultrasound cavitation and microfluidizer. Ultrason Sonochem. 20, 485–497. https://doi.org/10.1016/J.ULTSONCH.2012.04.005.
Tesař, V., Zhong, S., Rasheed, F., 2013. New fluidic-oscillator concept for flow-separation control. AIAA J. 51, 397–405. https://doi.org/10.2514/1.J051791.
Thaker, A.H., Ranade, V.V., 2021a. Drop breakage in a single-pass through vortex-based cavitation device: experiments and modeling. AIChE J. https://doi.org/10.1002/aic.17512.
Thaker, A.H., Ranade, V.V., 2022a. Emulsions using a vortex-based cavitation device: influence of number of passes, pressure drop, and device scale on droplet size distributions. Ind. Eng. Chem. Res 62, 18837–18851.

Thaker, A.H., Ranade, V.V., 2022b. Emulsions using a vortex-based cavitation device: influence of number of passes, pressure drop, and device scale on droplet size distributions. Ind. Eng. Chem. Res. https://doi.org/10.1021/acs.iecr.2c03714.

Thaker, A.H., Ranade, V.V., 2023. Drop breakage in a single-pass through vortex-based cavitation device: experiments and modeling. AIChE J. 69, e17512 https://doi.org/10.1002/AIC.17512.

Thaker, A.H., Ranade, V.V., 2021b. Towards harnessing hydrodynamic cavitation for producing emulsions: breakage of an oil drop in a vortex based cavitation device. Chem. Eng. Process. - Process. Intensif., 108753 https://doi.org/10.1016/J.CEP.2021.108753.

Urban, K., Wagner, G., Schaffner, D., Röglin, D., Ulrich, J., 2006. Rotor-stator and disc systems for emulsification processes. Chem. Eng. Technol. 29, 24–31. https://doi.org/10.1002/ceat.200500304.

Wang, X., Jiang, Y., Wang, Y.W., Huang, M.T., Ho, C.T., Huang, Q., 2008. Enhancing anti-inflammation activity of curcumin through O/W nanoemulsions. Food Chem. 108, 419–424. https://doi.org/10.1016/J.FOODCHEM.2007.10.086.

Xiao, Q., Wang, J., Yang, N., Li, J., 2017. Simulation of the multiphase flow in bubble columns with stability-constrained multi-fluid CFD models. Chem. Eng. J. 329, 88–99. https://doi.org/10.1016/J.CEJ.2017.06.008.

Zhang, Z., Wang, G., Nie, Y., Ji, J., 2016. Hydrodynamic cavitation as an efficient method for the formation of sub-100 nm O/W emulsions with high stability. Chin. J. Chem. Eng. 24, 1477–1480. https://doi.org/10.1016/J.CJCHE.2016.04.011.